Section - II

PERCUTANEOUS DRUG DELIVERY

Introduction

Non-steroidal anti-inflammatory drug (NSAIDs) is a class of drugs used for the treatment of rheumatoid arthritis (RA) and osteoarthritis (OA). Oral therapy of these agents is very effective, but their clinical use is often limited due to potential adverse effects.[1] The well known side effects of NSAIDs such as ulceration and irritation of gastrointestinal (GI) mucosa have accelerated the development of alternative delivery systems such as topical formulations that allow local absorption at the target tissue without systemic side effects. But to deliver the drug through skin is not an easy task due to the protective function of skin which poses physicochemical limitations to the permeant crossing the barrier. Special physicochemical requirements of the drugs for percutaneous delivery have limited the number of commercially available products based on topical drug delivery.

Various strategies have been developed over the years to improve percutaneous delivery of NSAIDs, and chemical modification of the drugs is one of them.[2] The present work is related to the development of novel percutaneous chemical drug delivery systems of some NSAIDs for the treatment of rheumatic diseases, So, it is in order to explain the principles of percutaneous delivery system in brief.

1. Percutaneous drug delivery systems

Percutaneous drug delivery means drug delivery through skin. It is a convenient route of drug administration which is acceptable by the patients. Ideally, drugs which need low doses or have high potency can be administered through the skin. Percutaneous drug delivery is mainly classified into two types:

1.1 Topical drug delivery

1.2 Transdermal drug delivery

1.1 Topical drug delivery

Topical delivery can be defined as application of a drug or drug containing formulation for the treatment of dermal, local soft tissue, and joint disorders. Topical approach is useful when the disease is associated with the skin or joint and for that the drug need to permeate into the skin and not to penetrate into blood circulation.[3]

1.2 Transdermal drug delivery

Transdermal drug delivery is the delivery of drugs through the skin to achieve a systemic effect. Objective of transdermal delivery is to avoid first pass metabolism and avoid side effects when administered by oral route.

1.3 Benefits of percutaneous drug delivery[4]

Percutaneous drug delivery possesses many advantages such as it avoids first pass metabolism and other variables such as low *p*H of the stomach, gastric emptying time etc. It provides sustained and controlled delivery of the drug, reduces systemic toxicity of the drug due to direct access to the target site, provides large surface area and a convenient route of administration of the drug. It is painless administration and has improved patient acceptance.

1.4 Limitations of percutaneous drug delivery[5]

Percutaneous delivery of drugs suffers from certain drawbacks such as the drug should have molecular weight less than 500 Da, its partition coefficient should be in between 1-3, may lead to pre-systemic metabolism of the drug due to presence of enzymes in the skin and may lead to side effects like skin irritation and sensitization reactions. Further, skin acts as an efficient barrier against absorption of large number of drugs.

2. Percutaneous drug delivery and skin

The major problem associated with percutaneous drug delivery is the excellent barrier property of the skin. In order to utilize successfully the phenomenon of percutaneous absorption it is necessary to understand the structure of the skin and its functions.

2.1 Structure of the skin

The skin is the largest organ in the body, comprising about 15% of the body weight. The total skin surface of an adult ranges from 12 to 20 square feet. In terms of chemical composition, the skin has about 70 % water, 25 % protein and 2 % lipids. The remainder includes trace minerals, nucleic acids, glycosoaminoglycans, proteoglycans and numerous other chemicals. The skin consists of three main layers: epidermis, dermis and subcutaneous tissue.[6] Cross section of the skin showing all the layers are shown in **Fig. 1.1.**

2.1.1 Epidermis

The epidermis is the topmost layer of the skin. Epidermis is classified in to two types, non-viable epidermis (stratum corneum) and viable epidermis (aqueous nature). The stratum corneum (SC) consists of multilayers of dead cells, hardened proteins (keratins), and lipids. Cells are flattened, compacted, dehydrated and keratinized forming a protective crust. Dead cells from stratum corneum continuously slough off and are replaced by new ones coming from below.[7]

The epidermis consists of three types of cells, keratinocytes, melanocytes and Langerhans cells. Keratinocytes, the cells that make the protein keratin, are the predominant type of cells in the epidermis. The skin completely renews itself every 3-5 weeks. Another significant group of cells in the epidermis is melanocytes, the cells producing melanin. The aqueous nature of the viable epidermis becomes the main barrier to percutaneous absorption of highly lipophilic drugs that have poor partitioning affinity towards an aqueous environment.[16]

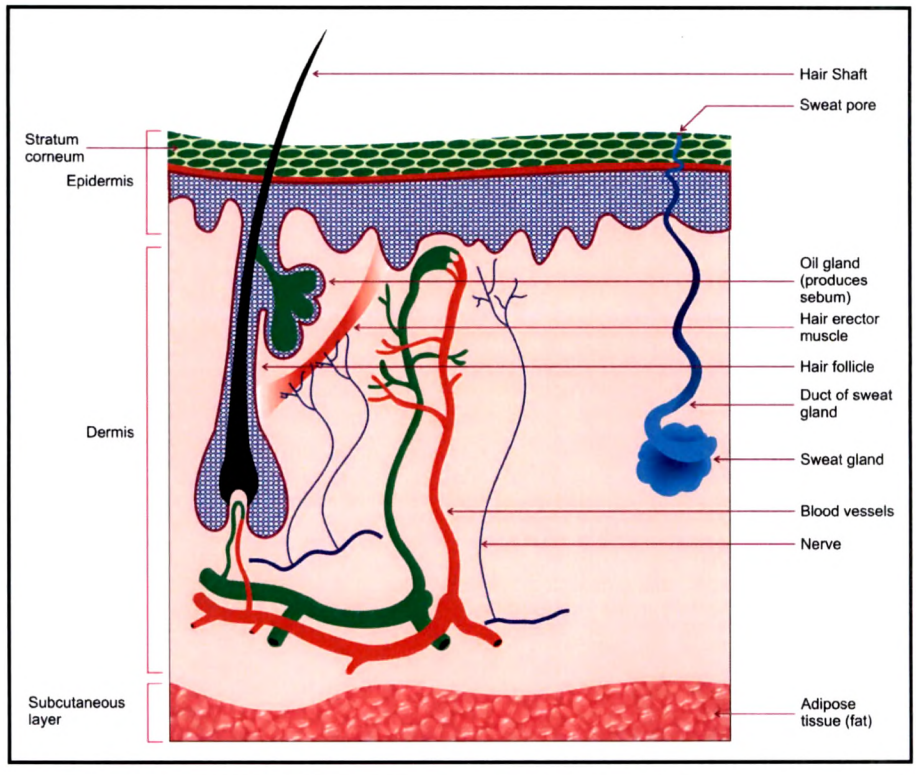

Fig.1.1: Cross section of human Skin

2.1.2 Dermis

The dermis is the middle layer of the skin located between the epidermis and subcutaneous tissue. It is the thickest layer of the skin (0.2-0.3 cm) and comprises a tight, sturdy mesh of collagen and embedded in amorphous colloidal ground substances such as elastin fibers. The key cells in the dermis are fibroblasts, which synthesize collagen, elastin and other structural molecules. The proper functioning of fibroblasts is highly important for overall skin health.[8]

The dermis also contains blood vessels, sensory nerves and lymph nodes. These are important for oxygenating and nourishing the skin and protecting it from invading microorganisms etc. It also contains segments of sebaceous glands, sweat glands, hair

follicles as well as a relatively small number of nerve and muscle cells. Sebacious glands, located around hair follicles, is of particular importance for skin health as they produce sebum, an oily protective substance that lubricates and waterproofs the skin and hair. The dermis is the layer responsible for the skin's structural integrity, elasticity and resilience.[9]

2.1.3 Subcutaneous tissue

Subcutaneous (hypodermis) tissue is the innermost layer of the skin located under the dermis and consists mainly of fat. The predominant type of cells in the subcutaneous tissue is adipocytes or fat cells.[10] Subcutaneous fat acts as a shock absorber and heat insulator, protecting underlying tissues from cold and mechanical trauma and provides cushioning to epidermis and dermis.

2.1.4 Skin appendages

There are various types of appendages on skin surface that include hair follicles with sebaceous gland, eccrine and apocrine sweat glands. There are about 40-70 hair follicles and 200-250 sweat ducts/cm^2 of the skin. The eccrine sweat glands (2-5 million) produce sweat (*p*H 4-6.8) and excrete several drugs, proteins and also control heat.

2.2 Functions of the skin[11-12]: Skin performs many functions as given below:

- It causes protection from water loss, injury, chemicals and microorganisms.
- It is responsible for excretion of urea and uric acid.
- It regulates body temperature,
- Skin helps in vitamin-D synthesis for body, has large blood reservoir and performs immunity functions against various allergens.

3. Drug permeation routes through skin

The process of percutaneous absorption is defined as the movement of substance(s) from the skin surface to the target tissue or general circulation. It involves penetration through the stratum corneum, diffusion through layers of skin, uptake by capillary network and finally transportation to the target tissues to achieve therapeutic action.

As shown in **Fig. 1.2.** there are four routes by which drugs can permeate the skin, which includes:[13-15]

3.1. Transappendageal (follicular) route: permeation through hair follicles

3.2. Transcellular (intracellular) route: permeation through cells

3.3. Paracellular route (intercellular route): It is the major route for the drug permeation and involves permeation of drug in between cells.

3.4. Appendageal route (eccrine): permeation through sweat gland, eccrine gland.

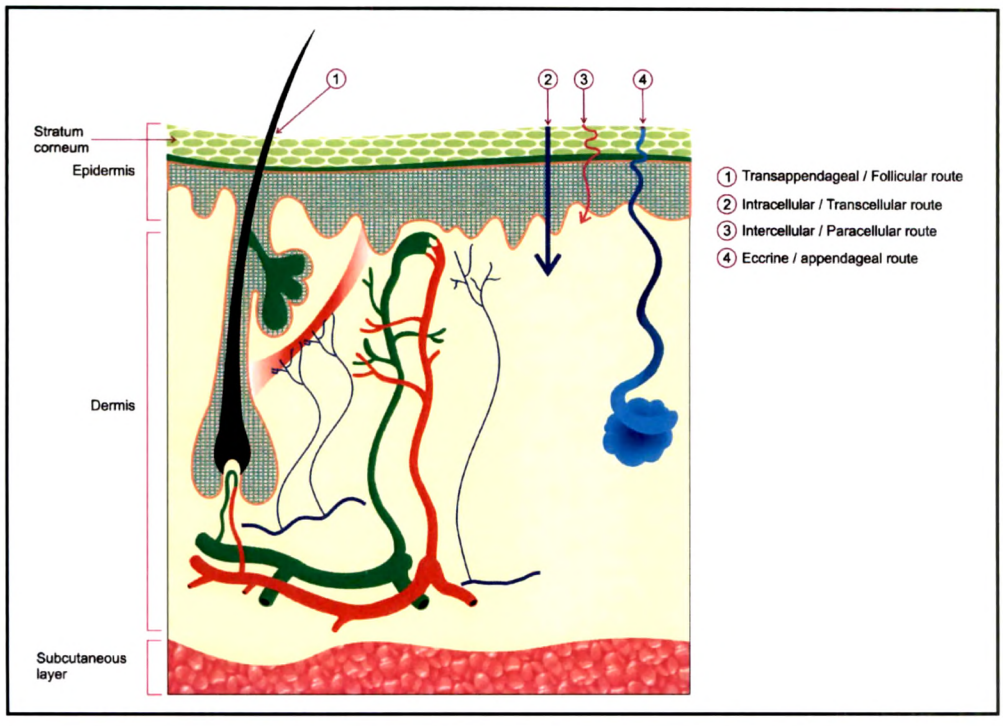

Fig. 1.2: Possible drug permeation routes across human skin

4. Pharmacokinetics of drugs through skin

The phenomenon of permeation by diffusion of the permeant into and through the skin and finally into the blood stream is known as percutaneous absorption.[16] Before a topically applied drug can act either locally or systemically, it must permeate the skin. The process of percutaneous absorption is complicated and involves a large number of processes occurring either consequently or simultaneously.[17] However, the current knowledge of percutaneous absorption involves mainly six steps which must occur before a drug can be absorbed from a topically applied formulation and ultimately appear in the cutaneous circulation or deeper tissues:[18]

1) The drug transports (dissolution) within the delivery system to vehicle-skin surface interface.
2) Partitioning of the drug takes place from the vehicle in to the SC.
3) There occurs diffusion of the drug through the SC.
4) Partitioning of the drug from the lipophilic SC into the aqueous viable epidermis takes place.
5) Diffusion of the drug takes place through the viable epidermis and upper dermis.
6) Ultimately there is drug uptake by cutaneous circulation.

Passive diffusion is the primary process for the drug permeability through skin. Therefore the general phenomenon of skin permeation can be described by the Fick's law of diffusion, which offers the basis for the development of the equation for drug absorption.[16, 19-20] *In vitro* skin permeation studies are often carried out by using diffusion models where a membrane is placed between two compartments; the drug formulation is placed in one compartment while the other compartment has a receptor solution providing sink conditions. After sufficient time, steady state diffusion across the membrane prevails and Fick's law of diffusion is expressed as follow:

$$J_{ss} = \mathbf{DCo/h} \text{---------- (1)}$$

Where J_{ss} is the steady state rate of the skin permeation; **D** is diffusion coefficient of permeation within the membrane; **Co** is the concentration of the permeation in the first layer of the membrane on the donor side and **h** is effective thickness of membrane.

The concentration **Co** within the membrane is difficult to measure, but the Co is related to **C**, the concentration of permeant in the donor phase that baths the membrane, in accordance with the partition coefficient **P**. Thus, the steady state transport of a drug through a membrane per unit area can be expressed as an expanded form of Fick's law i.e.:

$$J_{ss} = \mathbf{DPC/h} \text{---------- (2)}$$

Where *Jss*= Steady state rate of skin permeation (rate of movement of permeant across the skin)

D= Diffusion coefficient of the permeant within the membrane

C= dissolved concentration of drug in vehicle (effective, donor side)

P= partition coefficient of permeant between the membrane and the vehicle

h= effective thickness of the membrane

. As complications and uncertainties remains upon exact determination of the vehicle/membrane partition coefficient and thickness of the membrane, it is useful to determine the permeability coefficient **K*p*** according to equation given below:

$$\mathbf{K}p = \mathbf{DP/h} \text{---------- (3)}$$

This can be substituted into equation (2) to give equation (4)

$$J_{ss} = \mathbf{K}p\mathbf{C} \text{---------- (4)}$$

Where the rate of movement of the permeant (J_{ss}) across the skin is directly proportional to the concentration gradient. The permeability coefficient **(Kp)** obtained experimentally, provides a means of expressing absorption measurements for comparing different concentrations.

Extrapolation of the pseudo steady state portion of the graph is given by equation (2) to the intercept on the axis providing a measure of lag time (t_L). The lag time is the time required for a permeant to establish a uniform concentration gradient with the membrane of thickness **h** having diffusion coefficient D as shown in equation (5)

$$t_L = h^2/6D \text{---------- (5)}$$

It should be noted that the Fick's law of diffusion is applied only to a simple, inert membrane and thus, it may be an over simplification of complex permeation processes actually taking place in SC as it excludes binding and metabolism of drugs in the skin.

5. Physicochemical properties of the drug affecting skin permeation

5.1 Partition coefficient (*P*)

Partition coefficient is defined as the ratio of the concentrations of the compound in organic phase (hydrophobic phase) and aqueous phase (hydrophilic phase). It is a useful parameter for determining the drug permeation into skin. Normally for determining partition coefficient 1-octanol is chosen as hydrophobic phase and water as hydrophilic phase.[21] The logarithm of the ratio of the concentrations of the solute in these two phases is called log*P*. For effective permeation through the skin the drug should have partition coefficient (log*P*) in between 1-3.

5.2 Diffusion coefficient (*D*)

Fick's first law of diffusion states that flux of the solute goes from the higher concentration to lower concentration. Magnitude of the flux is directly proportional to the concentration gradient. Fick's first law relates with the assumption of flux of the solute in steady state.[22]

5.3 Balanced hydrophilic-lipophilic characteristics

Very lipophilic compounds may be retained in the SC which results in limited permeation into the aqueous viable epidermis. So ideally a compound must possess balanced hydrophilic and lipophilic properties.[23]

5.4 Drug concentration

Increase in concentration of the drug in vehicle increases its percutaneous absorption. At a constant drug concentration, the amount absorbed is directly proportional to the surface area. However this is not applicable to all drugs; few drugs produce significant decrease in absorption rates with increase in concentration.[24,28]

5.5 Interaction between skin, drug and vehicle

Rate of drug permeation through skin is influenced by interactions between drug-skin, drug-vehicle and vehicle-skin. A drug-skin interaction may result in increase or decrease in penetration rate of the drug, Vehicle-skin interaction may change hydration state of the SC and may change skin permeability. Drug-vehicle interaction results in slow diffusion of the drug from the vehicle on to the skin surface and decrease in skin permeability.[25,28]

5.6 Solubility and molecular characteristics of drug

Aqueous solubility of a drug strongly influences the rate of transport across the absorption site. Increase in solubility increases the skin permeation rates but there should be a balance between hydrophilic and lipophilic properties of molecules. It has been proved that skin permeation rate increases in presence of fatty acids and amines.[26]

5.7 Degree of ionization

Lipophilic nature of biological membranes allows unionized molecules to permeate easily. Ionized species were 10^4 times less permeable than unionized species. However it has been suggested that ionized species can permeate the lipid membranes through pores (like GIT). Various *in vitro* studies have shown that both ionized and unionized species of a drug can permeate a lipid membrane.[27]

5.8 Other factors

Other parameters which affect permeability through skin include effect of vehicle/solvent, degree of skin hydration, skin temperature, skin age and regional sites, species variation, pathological injuries to the skin, cutaneous drug metabolism, polymorphism, viscosity, surface tension, volatility of solvent, particle size etc. All these parameters affect skin permeation. Further, compounds with lower melting points have better skin permeation.[28]

6. Percutaneous drug delivery of NSAIDs

Various guidelines for percutaneous NSAIDs were developed through a regimented process of systematic review of the literature and are evidence based. **Table 1.1** enlists current OA guidelines. These guidelines reflect the expertise of US, European and international physicians and researchers from a variety of medical disciplines.[29] All guidelines recommend use of topical NSAIDS except AHA scientific statement. The AHA scientific statement is focused more narrowly on minimizing cardiovascular risks and therefore differs from these guidelines in recommending paracetamol or NSAIDs.[29]

Table 1.1: Guideline with recommendations for topical NSAIDs [29]

No	Guideline	Recommendation
1	AGS	All patients with other localized non-neuropathic persistent pain may be candidates for topical NSAIDs
2	AAOS	Patients with symptomatic OA of the knee, history of ulcer, GI bleeding receive one of the following for pain 1. Acetaminophen (<4 g/day), 2. Topical NSAIDs, 3. NSAIDs plus gastroprotective agent, Cycloxygenase-2 inhibitors
3	AHA	None
4	OARSI	Topical NSAIDs and capsaicin can be effective and alternatives to oral analgesics/NSAIDs in knee OA
5	NICE	Consider topical NSAIDs for pain relief in addition to core treatment
6	EULAR	Local treatment is preferred over systemic treatments for mild-to-moderate pain and when only few joints are affected

AAOS: *American academy of orthropaedic surgeons;* **AGS**: *American geriatrics society;* **AHA**: *American heart association;* **EULAR**: *European league against rheumatism;* **NICE**: *National institute for health and clinical excellence;* **OARSI**: *Osteoarthritis research society international.*

The OARSI, EULAR and AGS guidelines recommend that physicians initial pharmacologic treatment with paracetamol and topical NSAIDs are appropriate candidates for second line therapy in patients who do not tolerate or respond to paracetamol. EULAR recommends that topical NSAIDs are safe and effective.

7. Strategies to improve percutaneous drug delivery

NSAIDs are widely used for the treatment of rheumatic diseases and related painful conditions but bioavailability of topically applied NSAIDs is only 1-2 %. To improve the percutaneous delivery of NSAIDs, various strategies have emerged over recent years and these can be categorized as shown in **Fig.1.3**.[30] Formulation and chemical modifications of the drugs are the two major approaches which are useful in targeting the drugs to cross the skin barrier function.

7.1 Formulation approach

Conventional formulation approach includes various types of formulations used for the topical drug delivery. Most commonly they incorporate the chemical permeation enhancers such as menthol, ethanol, isopropyl alcohol, limonene etc. which increase the permeability of drugs through skin but simultaneously increase skin irritation also. While newer formulations like liposomes, niosomes, ethosomes, transferosomes are also gaining importance, but they are much more expensive and not suitable for all the drugs.

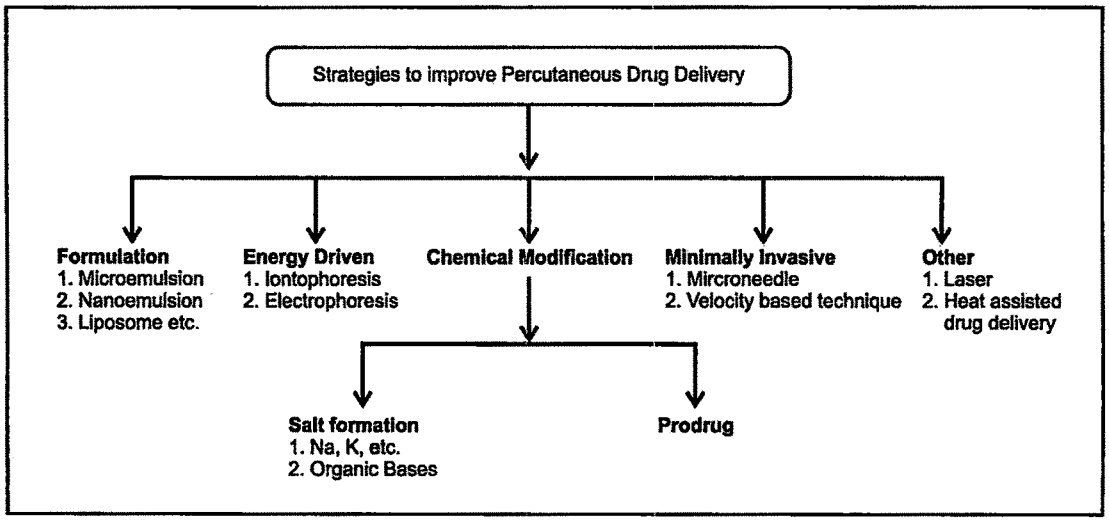

Fig. 1.3: Strategies for improving skin permeation of drugs

7.1.1 Microemulsions

A transdermal preparation containing ketoprofen was developed by Yun-Seok Rhee *et al.*[31] using o/w microemulsion system. The optimum formulation of the microemulsion consisted of 3% ketoprofen, 6 % oleic acid, 30 % Labrasol/ Cremophor (1:1) and water. Various terpenes (5 %) were added to the microemulsion and their effect on the skin permeation of ketoprofen from the microemulsion was evaluated. Limonene resulted 3-fold increase in enhancing activity over the control.

7.1.2 Nanoemulsions

Various o/w nanoemulsions of aceclofenac were prepared by Shakeel *et al.* [32] by the spontaneous emulsification method. A significant increase in permeability parameters such as steady-state flux (J_{ss}) and permeability coefficient (K*p*), were observed in optimized nanoemulsion formulation.

7.1.3 Liposomes

Liposomal formulation of naproxen was prepared for percutaneous drug delivery using different lipids such as stratum corneum lipids (SCL) and phosphatidylcholine/cholesterol (PC/CHOL). *In vitro* diffusion was studied by Franz diffusion cell on liposome dispersions viscosized by carbomer. The *in vitro* study showed a lower naproxen flux for stratum corneum lipids with respect to PC/CHOL liposomes. So, it is concluded that PC/CHOL liposome promoted naproxen permeation through the skin.[33]

2.2. Salt formation approach

For the percutaneous delivery of piroxicam (**1**), various ethanolamine salts (PX-EAs, **1a-1c**) were prepared to improve physicochemical properties for transdermal application. Piroxicam monoethanolamine salt (**1a**) and piroxicam diethanolamine salts (**1b**) had higher solubility than piroxicam in most of the vehicles tested and a higher permeation rate across the skin.[34]

The preparation of mefenamic acid alkanolamine salts (**2a-2d**) (monoethanolamine, diethanolamine, triethanolamine and propanolamine) was attempted to increase the transdermal flux of mefenamic acid.[35] A lipophilic enhancer system consisting of isopropyl myristate (IPM) and ethanol (9:1) produced a marked enhancement of mefenamic flux from the alkanolamine complexes through hairless rat skin membrane.

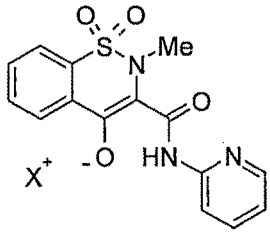

(1a-1c)

X^+ =

a= H_3N^+-CH_2CH_2OH

b= $H_2N^+(CH_2CH_2OH)_2$

c= $HN^+(CH_2CH_2OH)_3$

d= $H_2N^+CH_2CH_2CH_2OH$

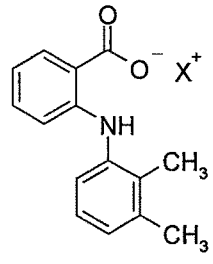

(2a-2d)

Among the alkanolamines examined, the propanolamine complex had the greatest enhancing effect on the permeation of mefenamic acid. So, the salt formation results in increased permeability as salts are more soluble in aqueous system than the drug alone.

2.3 Prodrug approach

K. B. Sloan *et al.* have synthesized *N,N*-dialkylhydroxylamine derivatives of indomethacin (**3a-3b**) to improve the delivery of indomethacin through mouse skin as

compared to indomethacin by a factor of two[37] which was found to be more effective than indomethacin in inhibiting thermal inflammation (two to three times) in animal models, but as effective as indomethacin in inhibiting UV radiation erythema in human volunteers. A series of acyloxyalkyl esters of ketoprofen **(4)** and naproxen **(5)** were synthesized by Rautio *et al.*[36] and investigated as topical prodrugs with the aim of improving the dermal delivery of these drugs.

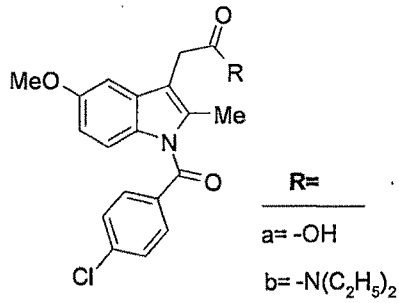

(3a-3b)

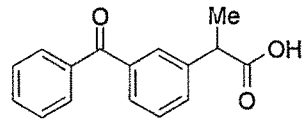

(4)

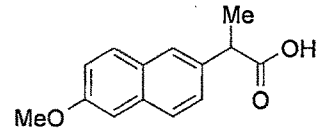

(5)

All acyloxyalkyl ester prodrugs (**6a-6h, 7a-7h**) were found to be much more lipophilic than their parent molecules, proved to be highly stable in aqueous solutions and hydrolyzed readily to the parent drugs both in human serum and human skin homogenate. However, the fluxes through excised human skin *in vitro* were still low, most probably due to poor aqueous solubility of the prodrugs and to high partition coefficients that were above the optimal range for skin permeation. Only the acetyloxyethyl ester prodrug of naproxen **(7e)**, which was the most hydrophilic member of the series, exhibited a slight enhancement of *in vitro* skin permeability compared to naproxen (**5**) itself.

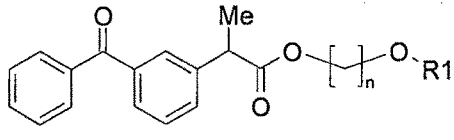

(6)

	n	R1
(6a)	2	-H
(6b)	3	-H
(6c)	4	-H
(6d)	1	$-COCH_3$
(6e)	2	$-COCH_3$
(6f)	3	$-COCH_3$
(6g)	4	$-COCH_3$
(6h)	1	$-COC(CH_3)_3$

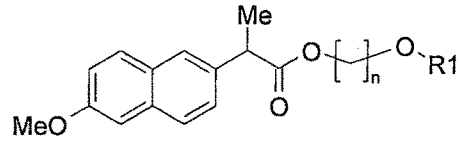

(7)

	n	R1
(7a)	2	-H
(7b)	3	-H
(7c)	4	-H
(7d)	1	$-COCH_3$
(7e)	2	$-COCH_3$
(7f)	3	$-COCH_3$
(7g)	4	$-COCH_3$
(7h)	1	$-COC(CH_3)_3$

Further, novel morpholinyl **(9a)** and piperazinylalkyl **(8, 9b** and **10a-10b)** esters of naproxen **(5)** were synthesized and evaluated *in vitro* for their properties as bioreversible topically administered dermal prodrugs **(5)** by Rautio *et. al.*[38]

Among the prodrugs, two piperazinyl derivatives **(9b)** and **(10b)** resulted in 4 and 9-fold enhancement of permeation compared to naproxen at *p*H 7.4. Further, novel polyoxyethylene esters of various NSAIDs were synthesized and evaluated as potential dermal prodrugs by Bonnia *et al.*[39]

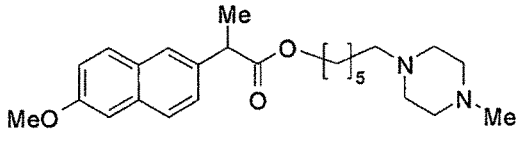

(8)

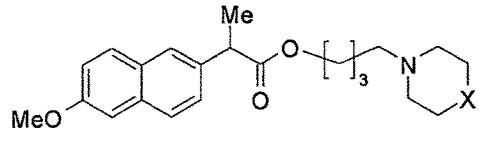

(9a) X= O
(9b) X= NCH_3

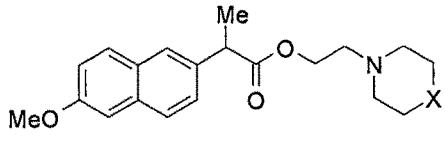

(10a) X= NH
(10b) X= NCH_3

Six 1-alkylazacycloalkan-2-one esters of ketoprofen **(14a-14c** and **15a-15c)** were synthesized and evaluated as potential dermal prodrugs of ketoprofen. Esters **(14a-14c** and **15a-15c)** showed increased lipophilicity compared with the parent drug ketoprofen **(4)**, and good stability in phosphate buffer (*p*H 7.4), and were readily hydrolyzed by porcine esterases.

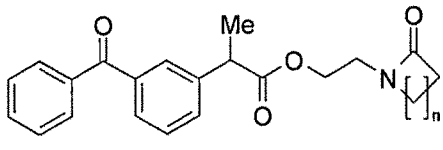

n=
(14a) = 1
(14b) = 2
(14c) = 3

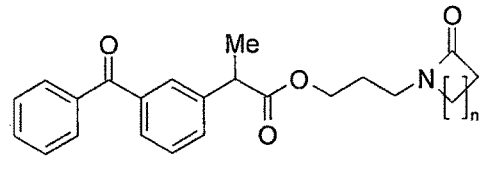

n=
(15a) = 1
(15b) = 2
(15c) = 3

Results from *in vitro* percutaneous absorption studies showed that, amongst all of the synthesized esters, only esters **(14a)** and **(15b)** showed higher cumulative amount of drug penetration through the skin, compared with that obtained after topical application of ketoprofen **(4)**. *In vivo* results showed an interesting delayed and sustained activity of ester **(15b)**, compared to the parent drug.[40]

From the literature survey it is concluded that dermal administration currently holds a high level of interest in pharmaceutical research. Literature also suggests that chemical modification i.e. salt formation and prodrug approach has big impact on permeability of NSAIDs as compared to other strategies to deliver NSAIDs by topical route.

References

1. Jelena D., Bozena M. and Kathryn E. U., Amphiphilic star like macromolecules as novel carriers for topical delivery of non-steroidal anti-inflammatory drugs. *AAPS Pharm. Sci.,* **2003**, 5, 1
2. Swarbrick J., Lee G., Brom J., Drug permeation through human skin. *J. Pharm. Sci.,* **1984**, 73, 1352-55
3. Marc B. B., Dermal and transdermal drug delivery systems. *Drug Deliv.* **2006**, 13, 175-187
4. Kim B.S., Won M., Lee K.M. and Kim C.S., *in vitro* Permeation studies of nanoemulsions containing ketoprofen as a model drug. *Drug. Deliv.,* **2008**, 15, 465-69
5. Rautio J., Synthesis and *in vitro* evaluation of topical prodrugs of some NSAIDs Ph.D. Thesis, Synthesis, University of kuopio, **2000**, P-16
6. Breathnach A.S. Aspects of epidermal ultrastructure. *J. Invest. Dermatol.*, **1975**, 65, 2-15
7. Odland G.F. Structure of the skin. In Goldsmith LA Ed. *Physiology, Biochemistry, and Molecular Biology of the Skin*, **1991**, 3-62
8. Lavker R.M. and Matoltsy A.G., Substructure of keratohyalin granules of the epidermis as revealed by high resolution electron microscopy. *J. Ultrastruct. Res.,* **1971**, 35, 575-81
9. Lynley A.M. and Dale B.A., The characterisation of human epidermal filaggrin, a histidine rich keratin filament-aggregating protein. *Biochim. Biophys. Acta.* **1983**, 744, 28-35
10. Rice R.H. and Green H., The cornified envelope of terminally differentiated human epidermal keratinocytes consists of cross-linked protein. *Cell.,* **1977**, 11, 417-22
11. Buxman M.M., Wuepper K.D., Cellular localization of epidermal trans-glutaminase: a histochemical and immunochemical study. *J. Histochem. Cytochem.*, **1978**, 26, 340-48
12. Handgraft J. Structure activity relationships and percutaneous absorption. *J. Control. Rel.,* **1991**, 15, 221-26

13. Cullander C., What are the pathways of iontophoretic current flow through mammalian skin? *Adv. Drug Del. Rev.*,**1992**, 9, 119-35
14. Barry B. W., Lipid protein partitioning theory of skin penetration enhancement. *J. control. Rel.*, **1991**, 15, 237-48.
15. Guy R.H. and Handgraft J., Mathematical models of percutaneous absorption: In percutaneous absorption mechanism-methodology drug delivery. Marcel Dekker Inc, New York. **1989**, 13-26.
16. Scheuplein R.J. and Blank I.H., Permeability of the skin. *Physiol. Rev.*, **1971**, 51, 702-47
17. Guy R.H., Hadgraft J. and Bucks D.A., Transdermal drug delivery and cutaneous metabolism. *Xenobiotica.*, **1987**, 17, 325-43.
18. Guy. R.H. Transdermal drug delivery: The ground rules are emerging. *Pharm. Int.*, **1985**, 5, 112-116.
19. Idron B., Percutaneous absorption. *J. Pharm. Sci.*, **1975**, 64, 901-924
20. Barry B.W., Mode of action o permeation enhancers in human skin. *J. Control. Rel.* **1987**, 6, 85-97
21. Kerr D. Roberts W., 7-Alkylcarbonyloxymethyl prodrugs of theophylline. *Int. J. Pharm.*, **1998**, 167, 37-48
22. Guy R.H. and Handgraft J., Percutaneous penetration enhancement: Physicochemical considerations and implications for prodrug design in prodrugs: Topical and ocular drug delivery. Marcel Dekker Inc, New York. **1992**, 1-16.
23. Guy R.H., Handgraft J., Selection of drug candidate for transdermal drug delivery. In: Developmental issues and research initiative, Marcel Dekker Inc, New York. **1989**, 59-81.
24. Singh P. and Roberts M.S., Skin permeability and local tissue concentrations of nonsteroidal anti-inflammatory drugs after topical application. *J. Pharmacol. Exp. Ther.* **1994**, 268, 144-151
25. Moddaresi M., Brown M.B., Zhao Y., Tamburic S. and Jones S.A., The role of vehicle-nanoparticle interactions in topical drug delivery. *Int J Pharm.* **2010**, 400, 176-82
26. Montagna W., In The Evaluation of therapeutic agents and cosmetics, T. H. Stemberg and V. D. Newcomer, Eds., McGraw Hill, New York, **1964**
27. Copper E. R. Molecular modifications for dermal and transdermal drug delivery. *Pharm. Int.*, **1986**, 12, 308-10
28. Singh S. and Singh J., Transdermal drug delivery by passive diffusion and iontophoresis: A Review. *Med. Res. Rev.*, **1993**, 13, 569-621.

29. Roy D. A., New guidelines for topical NSAIDs in the osteoarthritis treatment paradigm. *Curr. Med. Res. Opin.*, **2010,** 26, 2871–76
30. Schuetz Y.B., Naik A., Guy R.H. and Kalia Y.N., Emerging strategies for the transdermal delivery of peptide and protein drugs. *Expert Opin. Drug Deliv.*, **2005**, 2, 533-38
31. Rhee Y.S., Choi J.G., Park E.S. and Chi S.C., Transdermal delivery of ketoprofen using microemulsions. *Inter. J. Pharm.*, **2001**, 228, 161-170
32. Faiyaz S., Sanjula B., Alka A., Javed A., Mohammed A. and Sheikh S., Nanoemulsions as vehicles for transdermal delivery of aceclofenac. *AAPS Pharm SciTech.*, **2007**, 8, 191-99
33. Puglia C., Bonina F., Rizza L., Cortesi R., Merlotti E., Drechsler M., Mariani P., Contado C., Ravani L. and Esposito E., Evaluation of Percutaneous Absorption of Naproxen from Different Liposomal Formulations. *J. Pharm. Sci.*, **2010**, 99, 2819-29
34. Hyun-Ah Cheong and Hoo-Kyun Choi., Enhanced percutaneous absoption of piroxicam via salt formation with ethanolamines. *Pharm. Res.*, **2002**, 19, 1375-80
35. Fang L., Numajiri S., Kobayashi D. and Morimoto Y., The use of complexation with alkanolamines to facilitate skin permeation of mefenamic acid. *Inter. J. Pharm.*, **2003**, 262, 13-22
36. Rautio J., Taipale H., Gynther J., Vepsalainen J., Nevalainen T. and Jarvinen T., *In Vitro* Evaluation of acyloxyalkyl esters as dermal prodrugs of ketoprofen and naproxen. *J. Pharm. Sci.*, **1998**, 87, 1622-28
37. K. B. Sloan et.al., Acyloxyamines as prodrugs of anti-inflammatory carboxylic acids for improved delivery through skin. *J. Pharm. Sci.* **1984**, 73, 1734-37
38. Rautio J., Nevalainen T., Taipale H., Vepsäläinen J., Gynther J., Laine K. and Järvinen T., Piperazinylalkyl prodrugs of naproxen improve *in vitro* skin permeation. *Eur. J. Pharm. Sci.*, **2000**, 11, 157-63
39. Bonina F.P., Puglia C., Barbuzzi T., de Caprariis P., Palagiano F., Rimoli M.G. and Saija A., *In vitro* and *in vivo* evaluation of polyoxyethylene esters as dermal prodrugs of ketoprofen, naproxen and diclofenac. *Eur. J. Pharm.Sci.*, **2001**, 14, 123-34
40. Bonina F., Santagati N.A. and Puglia C., Ketoprofen 1-alkylazacycloalkan-2-one esters as dermal prodrugs: i*n vivo* and i*n vitro* evaluations. *Drug. Dev. Ind. Pharm.* **2003**, 29, 181-90

2. Aims and Objectives

For the treatment of rheumatic diseases mainly RA and OA the percutaneous application of drugs has recently received considerable importance due to its advantages over other drug delivery methods.[1] In joint diseases the percutaneous delivery of drugs to underlying muscle and joints is of considerable importance. Evidence also supports that local application of NSAIDs induces less adverse effects than orally administered anti-inflammatory agents.[2-5] The bioavailability of topically applied NSAIDs is only up to 1-2% in humans.[1] This limitation has led to the development of various strategies to enhance permeation of drugs through skin that include salt formation, prodrug designing and formulation approaches. Besides low permeability, all NSAIDs have short half life (3-4 h) and other unsuitable physicochemical properties (log*P*, *p*Ka, molecular weight etc.)[5]

The objective of the present study was to investigate the usefulness of the salt formation and prodrug approaches to improve the percutaneous delivery of some NSAIDs such as 6-methoxy-2-naphthylacetic acid (6-MNA) **(16)** and biphenylacetic acid (BPA) **(17)** for the treatment of rheumatic diseases.

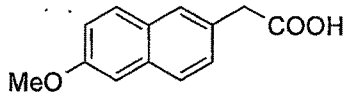

(16)

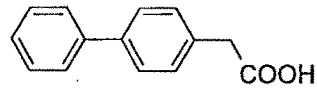

(17)

6-MNA and BPA are active metabolites of nabumetone and fenbufen respectively having long half life.[6-8]

Specific aims of the current work have been listed below:

1) Design of salts and prodrugs of 6-MNA and BPA to modify pharmacokinetic characteristics and thereby enhance the skin permeation.
2) Syntheses of the designed novel salts and prodrug derivatives of 6-MNA and BPA. These salts and derivatives are designed to release the parent drug via ionic bond cleavage (salts) or enzymatic and/or chemical hydrolysis of covalent bonds.
3) To evaluate the effects of promoieties on the physicochemical and kinetic properties of the prodrugs and salts; such as aqueous solubility, lipophilicity, chemical degradation or enzymatic hydrolysis and release of the parent drug.
4) To evaluate the effects of the physicochemical and kinetic properties of the synthesized prodrugs and salts for the *in vitro* skin permeation model.

5) To improve the skin permeation of 6-MNA and BPA through these prodrug and salt formation approaches.

References

1. Rautio J., Nevalainen T., Taipale H., Vepsäläinen J., Gynther J., Laine K. and Järvinen T., Synthesis and in vitro evaluation of novel morpholinyl and methyl piperazinyl acyloxyalkyl prodrugs of 2-(6-methoxy-2-naphthyl)propionic acid (Naproxen) for topical drug delivery. *J. Med. Chem.* **2000**, *43*, 1489-94
2. Suh H., Jun H.W., Dzimianski M.T. and Lu G.W., Pharmacokinetic and local tissue disposition studies of naproxen-following topical and systemic administration in dogs and rats. *Biopharm. Drug Dispos.* **1997**, 18, 623-33.
3. Underwood M., Advice to use topical or oral ibuprofen for chronic knee pain in older people: randomized controlled trial and patient preference study. *BMJ.* **2008**, 336, 138-42.
4. Altman R.D. New guidelines for topical NSAIDs in the osteoarthritis treatment paradigm. *Curr. Med. Res. Opin.* **2010**, 26, 2871-76
5. Rautio J., Nevalainen T., Taipale H., Vepsäläinen J., Gynther J., Laine K. and Järvinen T., Piperazinylalkyl prodrugs of naproxen improve in vitro skin permeation. *Eur. J. Pharm. Sci.* **2000**, 11, 157-63.
6. Roberts M.S. and Cross S.E., Percutaneous absorption of topically applied NSAIDS and other compounds: role of solute properties, skin physiology and delivery systems. *Inflammopharmacology.* **1999**, 7, 339-50.
7. Nobilis M., Kopecký J., Kvetina J., Svoboda Z., Pour M., Kunes J., Holcapek M. and Kolárová L., Comparative Biotransformation and Disposition Studies of Nabumetone in Humans and Mini pigs Using HPLC with Ultraviolet, Fluorescence and Mass-spectrometric Detection. *J. Pharm. Biomed. Anal.* **2003**, 32, 641-56
8. Brogden R.N., Heel R.C., Speight T.M. and Avery G.S., Fenbufen: a review of its pharmacological properties and therapeutic use in rheumatic diseases and acute pain. *Drugs.* **1981**, 21, 1-22.

3. Results and Discussion

The work carried out towards achieving the proposed plan has been classified in to the following two main headings:

3.1. Salt formation approach

3.2. Prodrug approach

3.1 Salt formation approach

The work has been discussed under the following three main headings:

3.1.1. Design of salts

3.1.2. Syntheses and characterization of salts

3.1.3. Physicochemical evaluation of the salts

3.1.3.1. Determination of aqueous solubility

3.1.3.2. Determination of Log *P*

3.1.3.3. *In vitro* skin permeation study

3.1.1 Design of salts

Salts are usually considered alternatives of the parent drugs for drug delivery systems if physicochemical properties of the parent drug molecules are not suitable for a formulation. As mentioned earlier all NSAIDs have very low permeability through skin (<1 %), short half life (3-4 h), and lack of affinity towards joints etc. Attempts have been made to improve their permeability by salt formation; however, none of the long acting salts of NSAIDs coupled with their specific affinity towards joints have been investigated till date.

In the current study various salts of active metabolites of nabumetone and fenbufen i.e 6-MNA **(16)** and BPA **(17)** respectively, have been designed, prepared and evaluated to improve their transdermal delivery for the treatment of arthritis. Considering the presence of acidic functional group we have designed some salts of these agents with organic and inorganic bases.

Alkanolamines such as ethanolamine, diethanolamine, triethanolamine and diethylamine (DEA) have been chosen for this purpose along with sodium salt. These agents are weak bases, and contain basic amino functional group and one or more polar hydroxyl groups except for the DEA and sodium salts. Amino group will react with acidic functional group present in the NSAIDs resulting into salt formation imparting aqueous solubility which is further enhanced by polar hydroxyl group. Structures of the designed salts are shown in **Fig. 3.1.1**

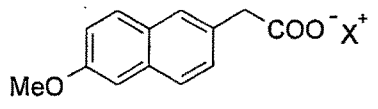

(18a-18e)

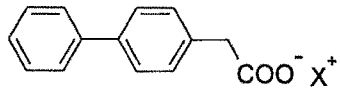

(19a-19e)

X^+ =

a: Na^+

+

b: $H_3N\text{-}CH_2CH_2OH$

+

c: $H_2N(CH_2CH_2OH)_2$

+

d: $HN(CH_2CH_2OH)_3$

+

e: $HN(CH_2CH_3)_2$

Fig. 3.1.1: The general structure of the designed salts of 6-MNA **(16)** and BPA **(17)**

3.1.2 Syntheses and characterization of the salts

6-MNA **(16)** and BPA **(17)** were dissolved separately in dichloromethane (wherever required small amount of methanol was added to make the solution clear) and an equimolar amount of base was added and the reaction mixtures were stirred for 6-8 h. The precipitated salts were collected by filtration and recrystallized from ethyl acetate to yield pure salts **(18a-18e)** and **(19a-19e)** of 6-MNA and BPA respectively.

Table 3.1.1: Physicochemical and spectral data of compounds **(16, 18a-18e)**

Compound	Physical State	Melting point (°C)	DSC (endotherm °C)	IR (cm^{-1})
16	White Solid	171-173	171.55	1693, 1416, 1265
18a	White Solid	>275	281.12	1707, 1267, 1028
18b	Yellow Solid	156-158	157.15	3285, 1704, 1263
18c	White Solid	72-74	80.01/117.38	3385, 1706, 1387
18d	White Solid	94-97	106.17	3354,1709, 1227
18e	White Solid	136-139	114.84	3389, 1707, 1264

Prepared salts were characterized by using IR and DSC. Physicochemical and spectral data of the compounds are listed in **Table 3.1.1** above, and the surface morphology was studied by SEM.

Regarding the interaction between 6-MNA and alkanolamine bases, important information was gathered from IR spectroscopy. The FT-IR spectra of 6-MNA and its

salts are shown in **Fig. 3.1.2.** 6-MNA showed a strong sharp signal at 1693cm^{-1}, characteristic of the carbonyl stretching vibrations.

The carbonyl peak of the 6-MNA in salt form was shifted to higher wavenumber (1707 cm^{-1}). Other signs of interaction were reflected by shifts in the range of 3389-3285 cm^{-1} due to N-H stretching which were absent in **16** and **18a**. However **18b** shows signals at 3285 cm^{-1} whereas **18c** and **18d** show peaks around 3385 cm^{-1} suggesting that the intermolecular hydrogen bonding of the salts might have shifted the N-H or O-H stretching bands.

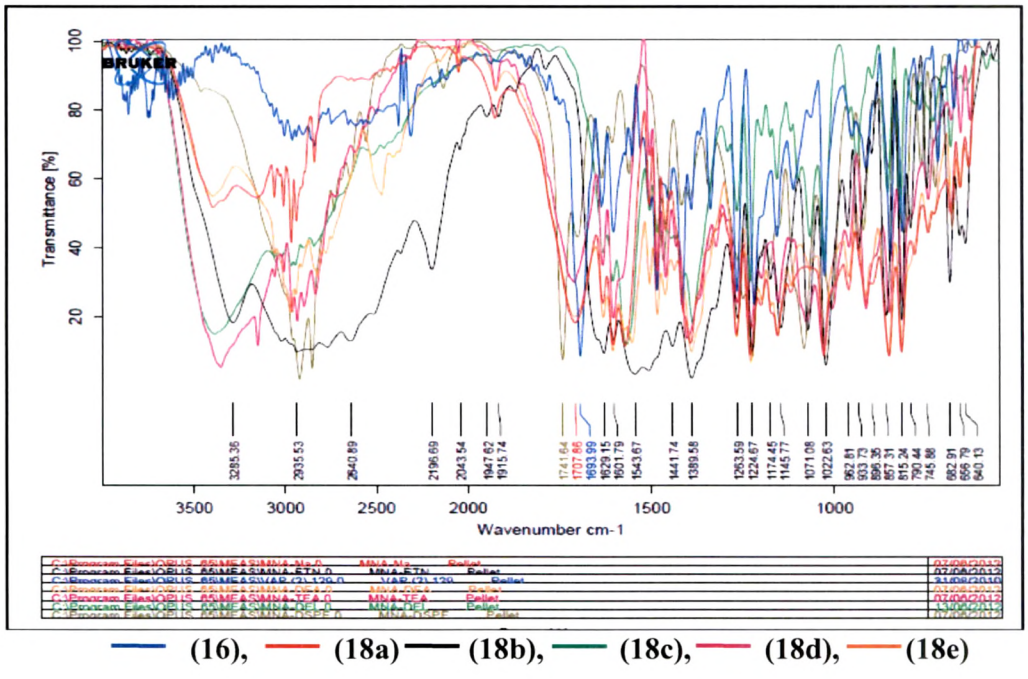

Fig. 3.1.2: Overlaid FT-IR Spectra of 6-MNA **(16)** and its salts **18a-18e)**

Fig. 3.1.3. and **3.1.4.** Show DSC curve of 6-MNA **(16)** and its salts **(18a-18e). Table 3.1.1** summarizes melting point and endothermic peaks of 6-MNA and its salts and these values are in good agreement with each other. Melting points of the salts decreased remarkably compared to the parent drug except for the sodium salt **(18a)** which showed higher melting point. All these shifts in melting points are indication of salt formation.

Surface morphology of the compounds vary from each other and to evaluate this parameter SEM of the prepared salts were performed. From this study we can conclude that each salt has a different surface morphology as shown in **Fig. 3.1.5.**

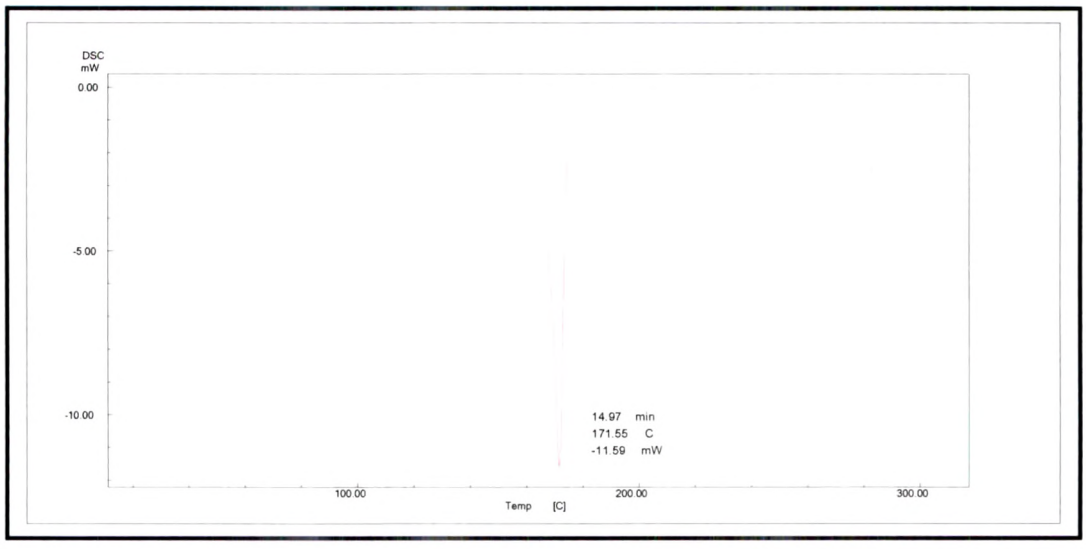

Fig. 3.1.3: DSC thermogram of 6-MNA **(16)**

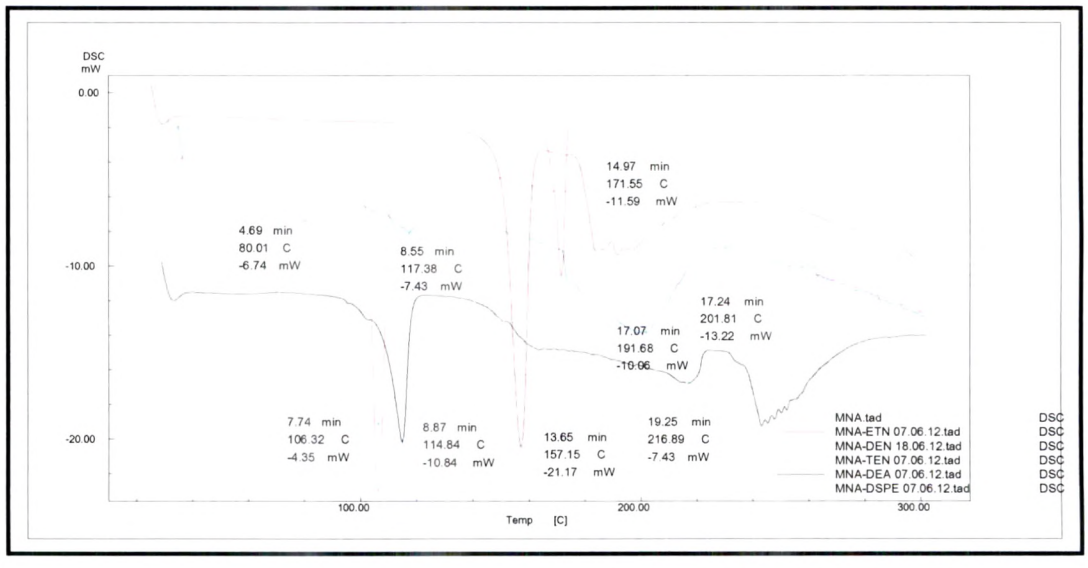

Fig. 3.1.4: Overlaid DSC thermograms of 6-MNA **(16)** and its salts **(18a-18e)**

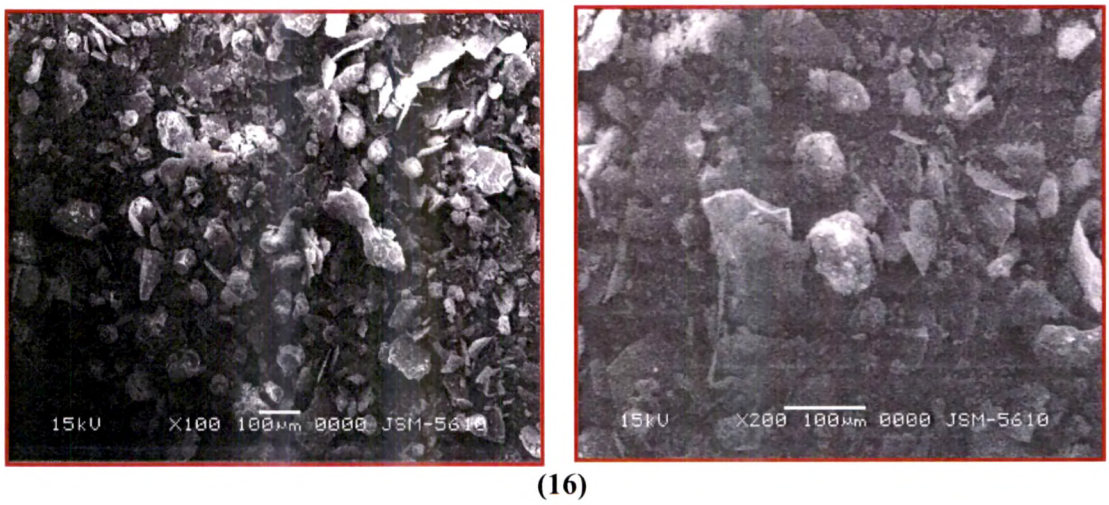

(16)

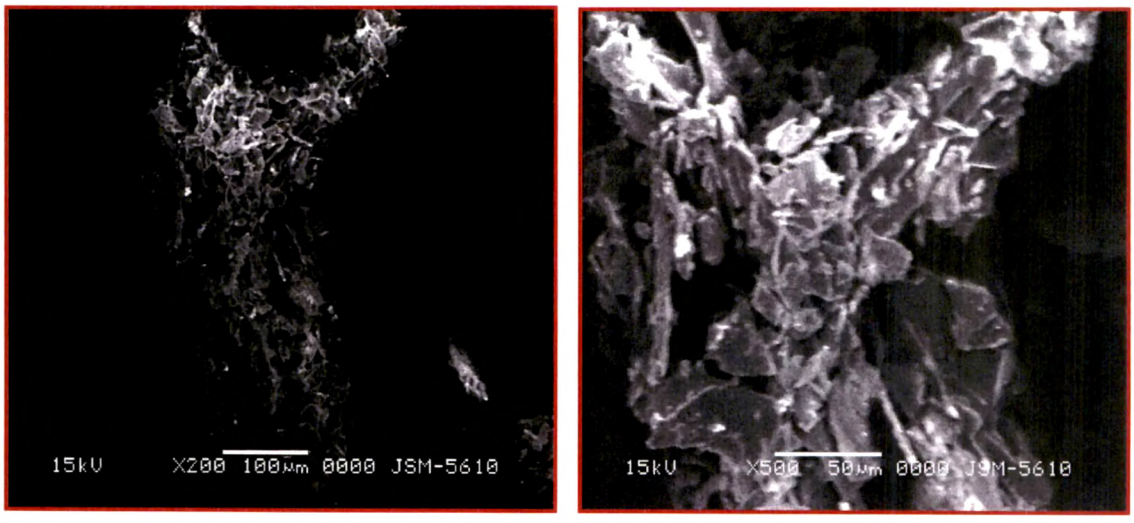
15kV X200 100µm 0000 JSM-5610
15kV X500 50µm 0000 JSM-5610

(18a)

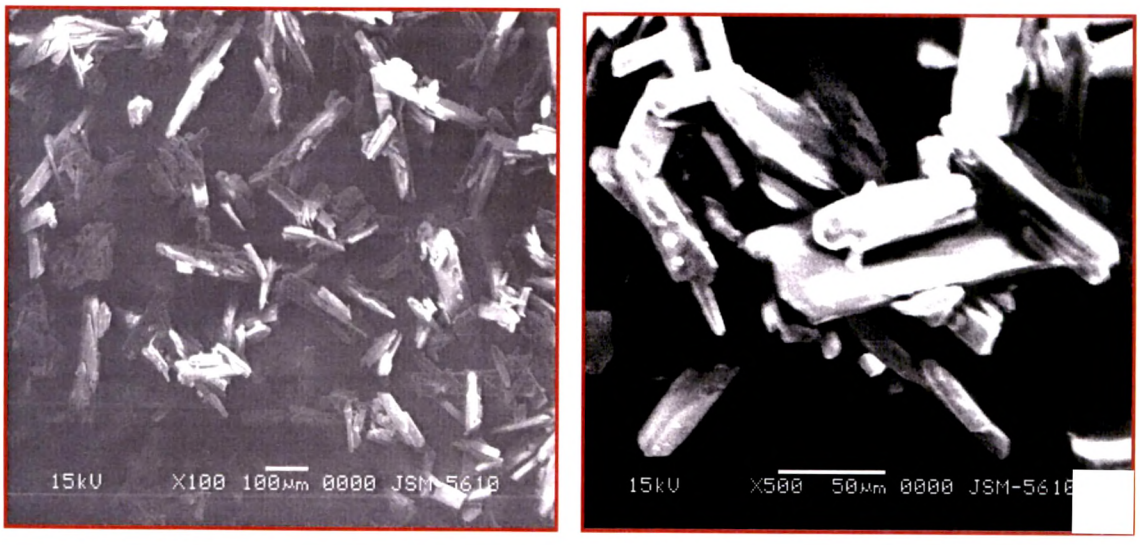
15kV X100 100µm 0000 JSM-5610
15kV X500 50µm 0000 JSM-5610

(18b)

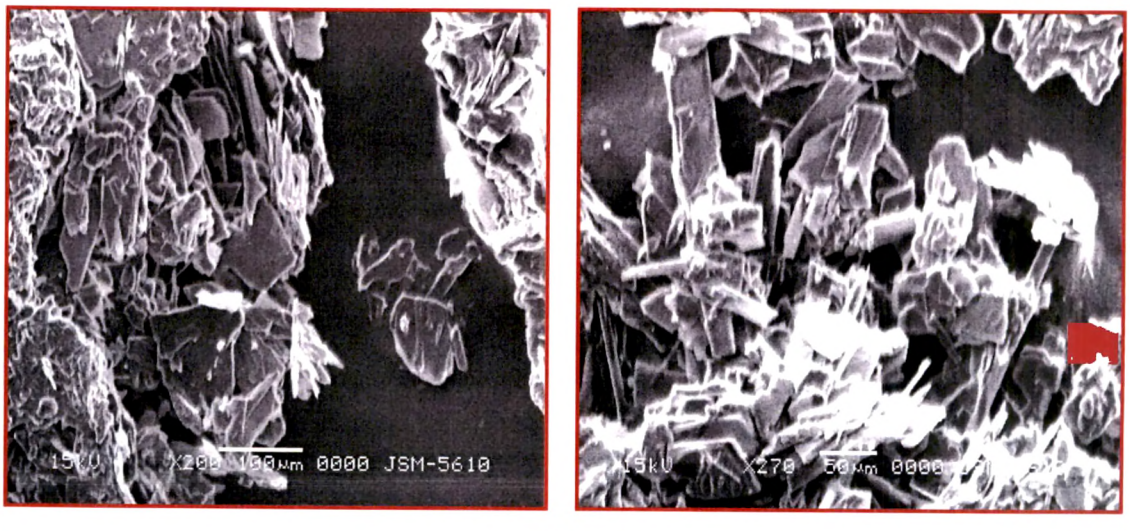
15kV X200 100µm 0000 JSM-5610

(18c)

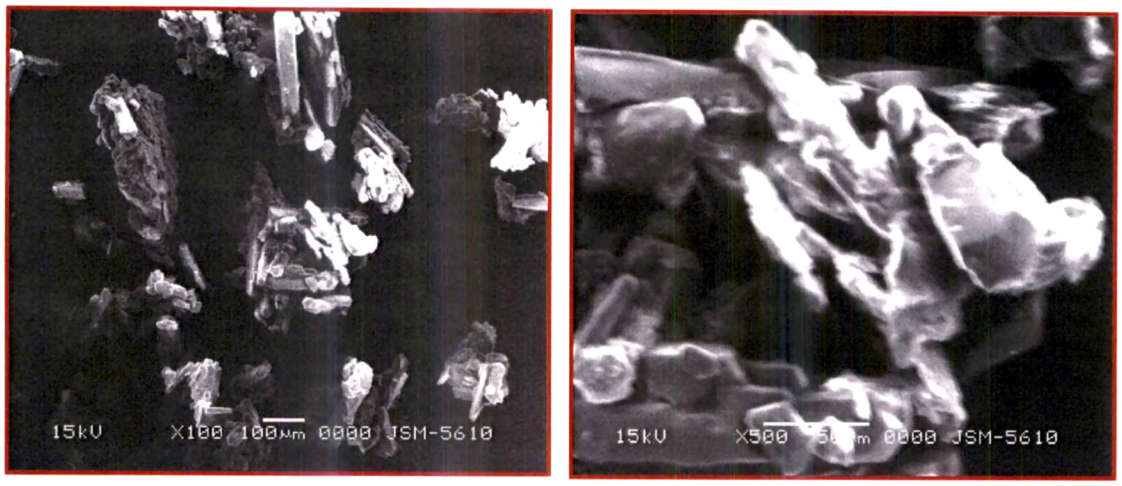

(18d)

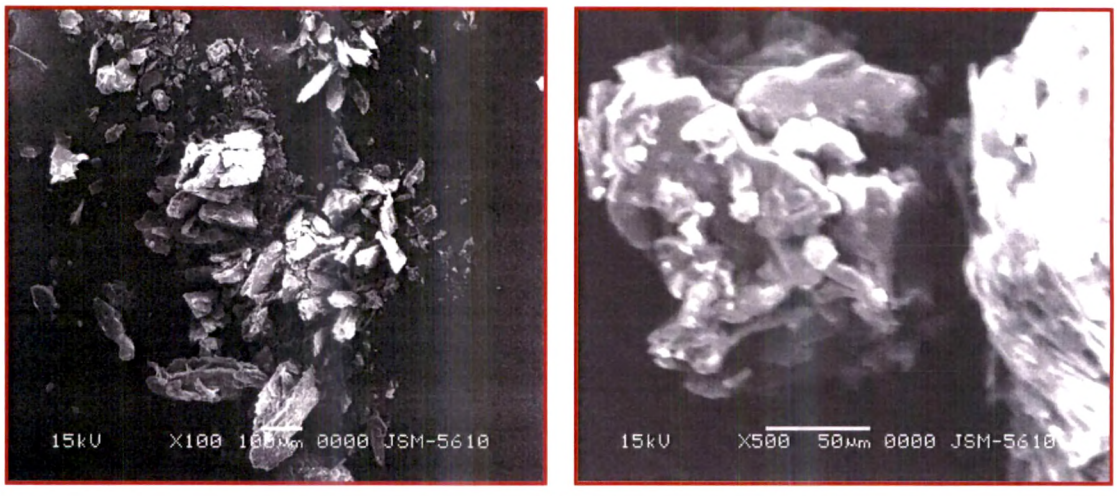

(18e)

Fig. 3.1.4: Scanning electron microscope images of compounds **(16, 18a-18e)**

Salts of BPA also show same features as described under 6-MNA **(16)**. The physicochemical and spectral data of compounds **(17, 19a-19e)** are shown in **Table 3.1.2.**

Table 3.1.2: Physicochemical and spectral data of compounds **(17, 19a-19e)**

Compound	Physical State	Melting point (^{o}C)	DSC (Endotherm^{o}C)	IR (cm^{-1})
17	White Solid	163-165	153.89	1685, 1413, 1249,
19a	White Solid	>275	--	1684, 1557, 1294,
19b	Yellow Solid	116-119	137.62	3263, 1674, 1391,
19c	Semisolid	--	--	3248, 1679, 1374,
19d	White Solid	82-84	87.91	3354, 1681, 1077,
19e	Semisolid	--	--	3407, 1699, 1571,

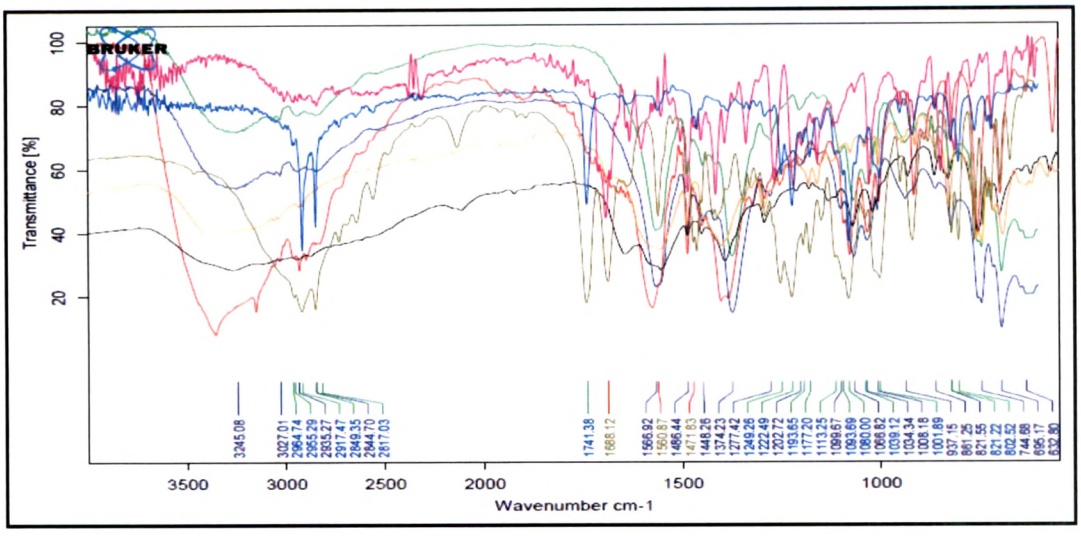

Fig. 3.1.6: Overlaid FT-IR Spectra of BPA **(17)** and its salts **19a-19e)**

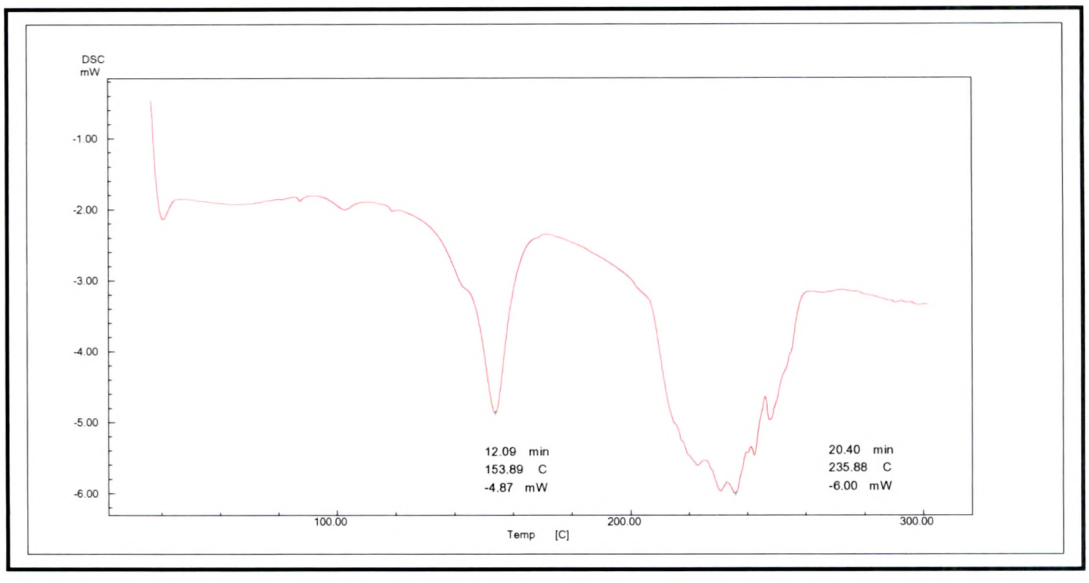

Fig. 3.1.7: DSC thermogram of BPA **(17)**

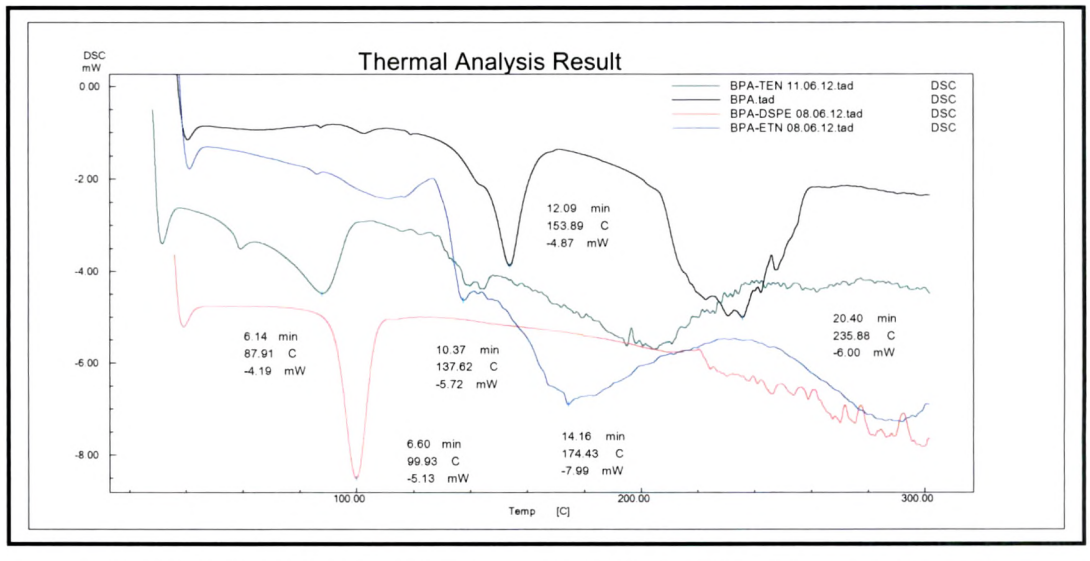

Fig. 3.1.8: Overlaid DSC thermograms of BPA **(17)** and its salts **19a-19e)**

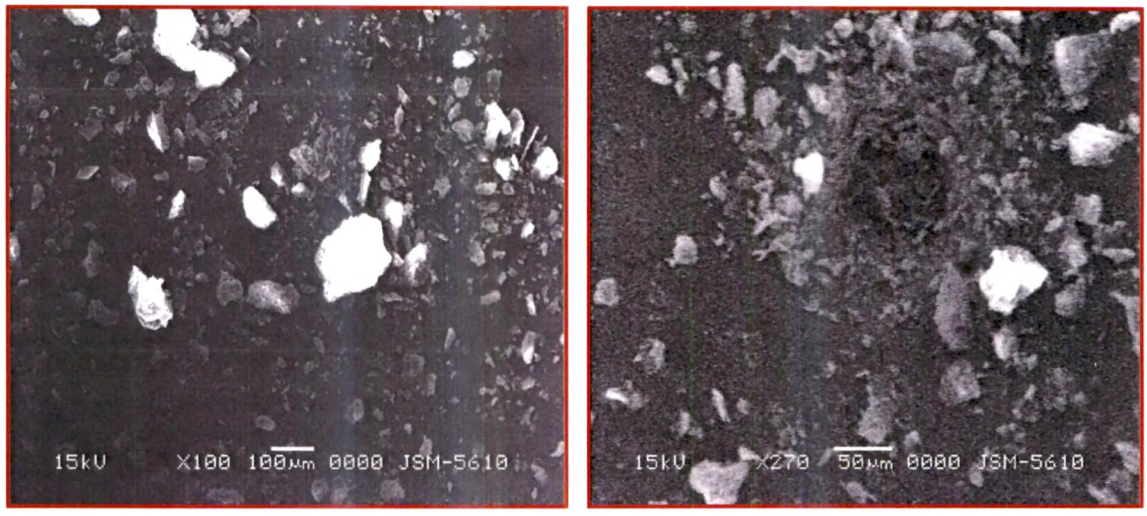
15kV X100 100µm 0000 JSM-5610
15kV X270 50µm 0000 JSM-5610

(17)

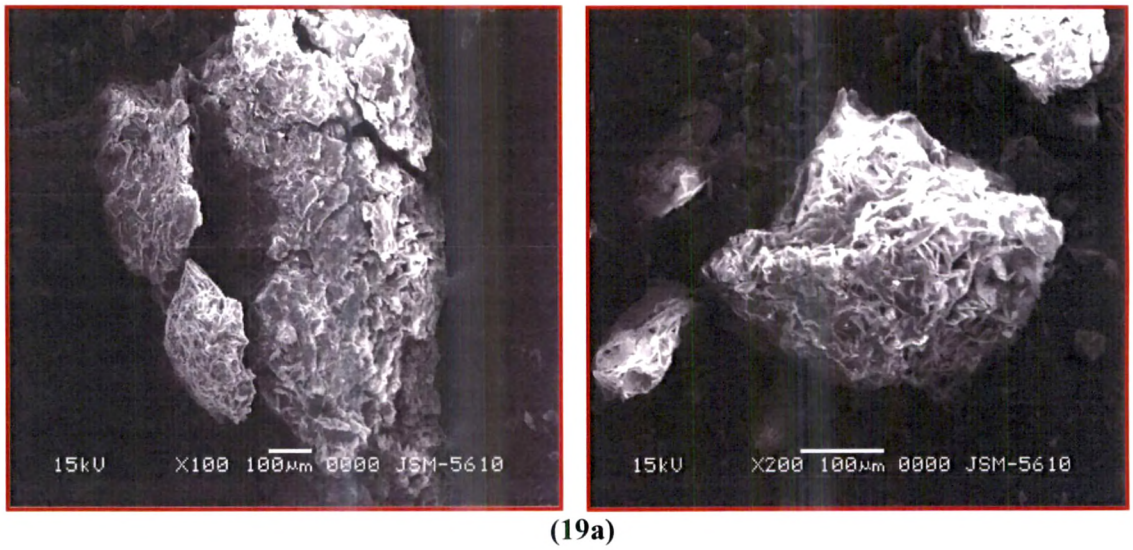
15kV X100 100µm 0000 JSM-5610
15kV X200 100µm 0000 JSM-5610

(19a)

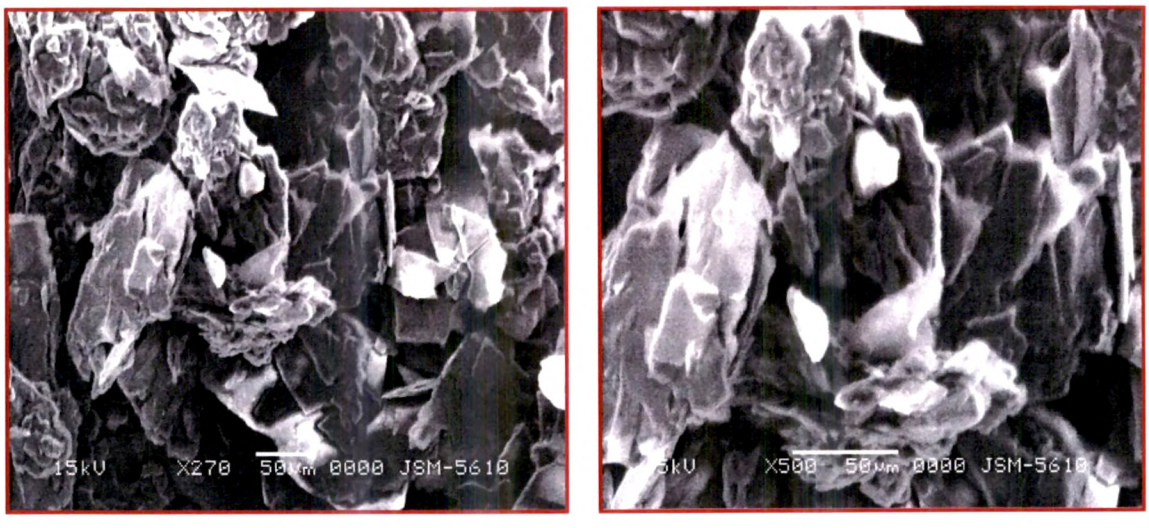
15kV X270 50µm 0000 JSM-5610
X500 50µm 0000 JSM-5610

(19b)

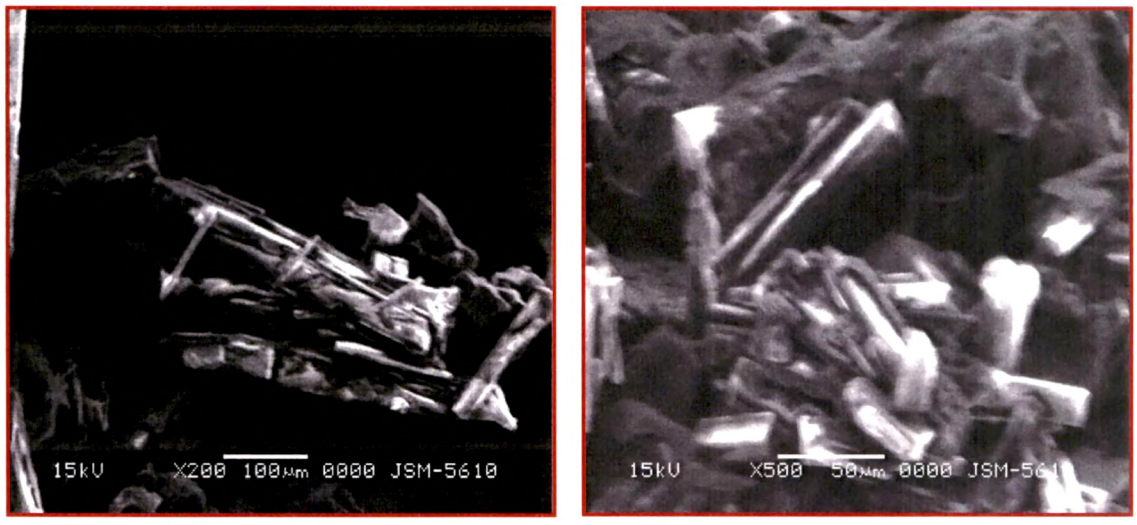

(19d)

Fig. 3.1.9: Scanning electron microscope images of compounds **(17, 19a-19d)**

3.1.3. Physicochemical evaluation

For the evaluation of various physicochemical parameters such as aqueous solubility, partition coefficient and *in vitro* skin permeability, HPLC method as developed earlier (Section-I) has been used. Calibration curves for 6-MNA **(16)** and BPA **(17)** were plotted and linearity range calculated.

3.1.3.1. Determination of aqueous solubility

Due to biphasic nature of skin, the ideal salt form should exhibit adequate lipid solubility as well as aqueous solubility. Aqueous solubility of 6-MNA and its salts were determined in phosphate buffer at the physiological *p*H 7.4 and at *p*H 5.0 as the environment of the outer surface of the skin is acidic (*p*H 4.2-6.5).[1,8] **Table 3.1.3** shows aqueous solubility of 6-MNA **(16)** and its salts **(18a-18e)**.

3.1.3.2. Determination of Log *P*

Lipid solubility plays a crucial role in determining skin permeability of a compound because the SC (stratum corneum) the major barrier to drug permeation is essentially lipoidal in nature and generally favors permeation of lipophilic drugs.[1] The apparent partition coefficients of 6-MNA **(17)** and salts **(18a-18e)** were determined by partitioning them between phosphate buffer (0.16 M) and saturated n-octanol at both *p*H 5.0 and *p*H 7.4 using shake flask method. **Table 3.1.4** shows Log P_{app} values of 6-MNA **(16)** and its salts **(18a-18e)**.

Table 3.1.3: Aqueous solubility of 6-MNA **(16)** and salts at *p*H 5.0 and at *p*H 7.4

Compound	Aqueous Solubility (mM)	
	***p*H 5.0**	***p*H 7.4**
16	0.78 ± 0.18	63.34 ± 0.24
18a	17.01 ± 0.19	24.08 ± 0.27
18b	34.81 ± 0.24	27.13 ± 0.29
18c	36.02 ± 0.31	31.09 ± 0.41
18d	21.92 ± 0.42	25.40 ± 0.72
18e	08.10 ± 0.29	06.09 ± 0.29

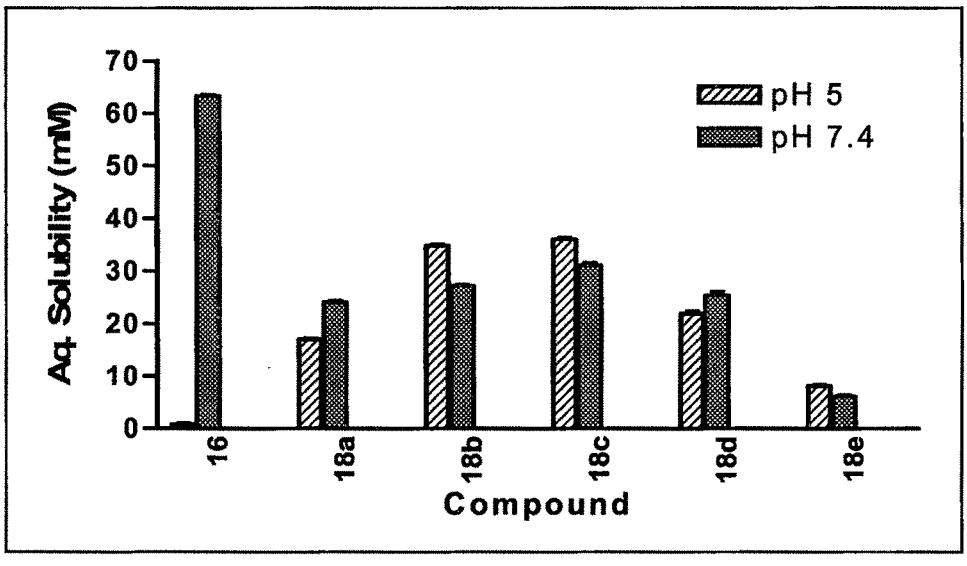

Fig. 3.1.10: Aqueous solubility of the 6-MNA **(16)** and salts **(18a-18e)** at *p*H 5.0 and at *p*H 7.4

Table 3.1.4: Partition coefficient (Log P_{app}) values of 6-MNA **(16)** and its salts

Compound	Log P_{app}	
	***p*H 5.0**	***p*H 7.4**
16	1.823 ± 0.020	0.233 ± 0.037
18a	0.807 ± 0.031	0.704 ± 0.061
18b	1.491 ± 0.041	1.063 ± 0.043
18c	0.917 ± 0.043	1.011 ± 0.031
18d	1.101 ± 0.015	1.061 ± 0.017
18e	2.310 ± 0.032	2.010 ± 0.019

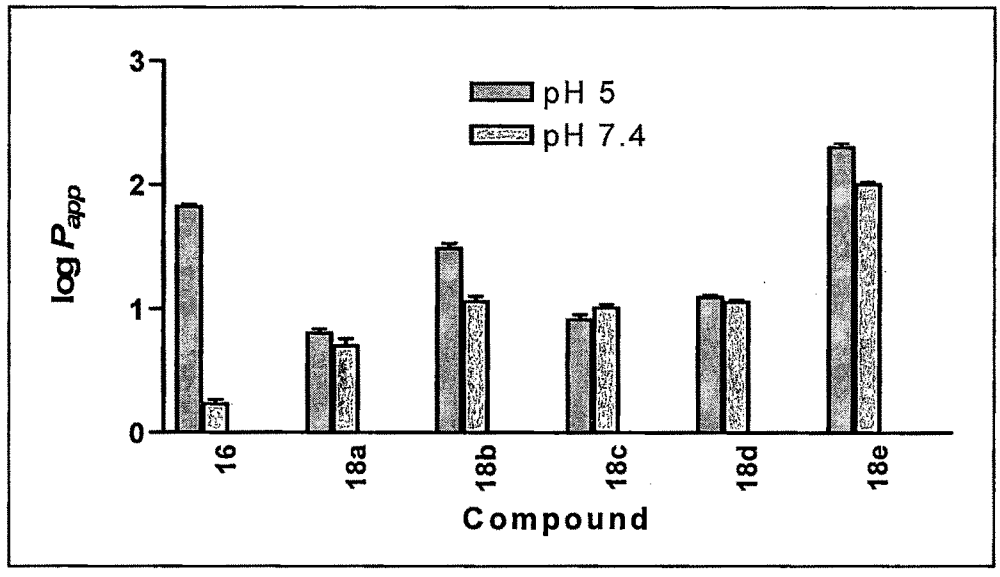

Fig. 3.1.11: Partition coefficient (Log P_{app}) values of 6-MNA **(16)** and its salts **(18a-18e)**

Table 3.1.5: Aqueous solubility of BPA **(17)** and salts at *p*H 5.0 and at *p*H 7.4

Compound	Aqueous Solubility (mM)	
	***p*H 5.0**	***p*H 7.4**
17	0.57 ± 0.14	54.08 ± 0.14
19a	14.23 ± 0.31	17.05 ± 0.21
19b	28.96 ± 0.28	24.10 ± 0.34
19c	41.05 ± 0.43	37.08 ± 0.33
19d	24.27 ± 0.22	21.30 ± 0.52
19e	07.20 ± 0.37	05.18 ± 0.45

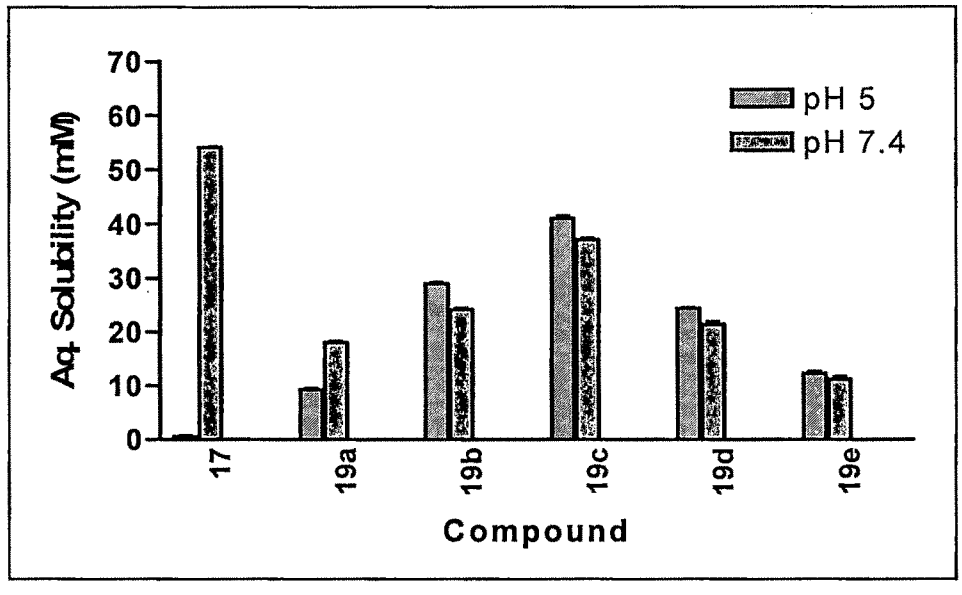

Fig. 3.1.12: Aqueous solubility of BPA **(17)** and its salts **(19a-19e)**

Table 3.1.6: Partition coefficient (Log P_{app}) values of BPA **(17)** and its salts

Compound	Log P_{app}	
	***p*H 5.0**	***p*H 7.4**
17	1.207 ± 0.060	0.433 ± 0.041
19a	0.687 ± 0.043	0.507 ± 0.052
19b	2.0340± 0.039	1.463 ± 0.076
19c	1.019 ± 0.073	0.911 ± 0.031
19d	1.208 ± 0.047	1.141 ± 0.047
19e	1.410 ± 0.031	1.010 ± 0.090

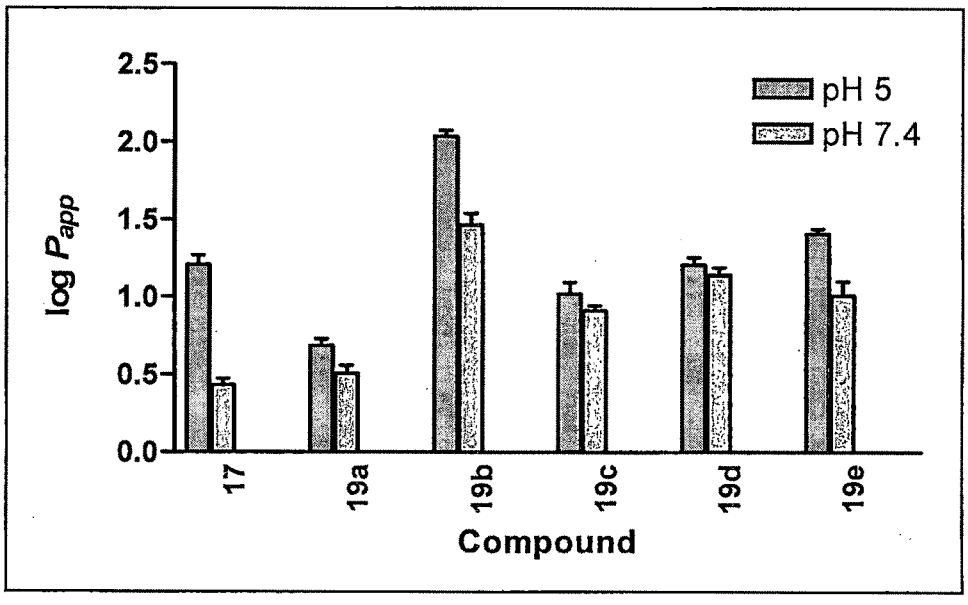

Fig. 3.1.13: Partition coefficient (Log P_{app}) values of BPA **(17)** and its salts **(19a-19e)**

3.1.3.3 *In vitro* skin permeation study

In vitro skin permeation study was performed by using rat skin. The *in vitro* diffusion experiments showed that salts of both 6-MNA **(16)** and BPA **(17)** were able to permeate rat abdominal skin. For each salt and parent drug the cumulative amounts permeated through skin were plotted against time. A steady state flux (*J*ss) was obtained by dividing the slope of that graph by surface area of the diffusion cell (4.906 cm^2).[1,8]

Table 3.1.7: *In vitro* skin permeation of 6-MNA **(16)** and its salts **(18a-18e)**

Time		Cumulative amount permeated (µg/cm^2)				
(h)	16	18a	18b	18c	18d	18e
1	3.85±2.0	9.87±3.0	15.55±2.0	7.69±3.0	6.04±2.0	5.34±2.0
2	6.81±2.0	19.13±3.0	36.88±4.0	18.55±2.0	11.08±2.0	9.01±3.0
4	16.01±3.0	45.75±4.0	109.4±5.0	64.61±5.0	29.88±4.0	19.44±4.0
8	29.49±4.0	84.66±5.0	215.1±7.0	164.06±9.0	67.4±5.0	61.7±8.0
24	52.96±5.0	252.62±9.0	450.4±14.0	356.4±16.0	176.8±11.0	148.6±10.0

Table 3.1.8: *In vitro* skin permeation of BPA **(17)** and its salts **(19a-19e)**

Time		Cumulative amount permeated (µg/cm^2)				
(h)	17	19a	19b	19c	19d	19e
1	3.46±2.0	12.05±3.0	28.47±2.0	22.14±3.0	18.7±2.0	9.58±2.0
2	6.66±2.0	23.45±3.0	61.51±4.0	57.44±2.0	38.1±2.0	19.45±3.0
4	18.51±3.0	56.81±4.0	157.89±5.0	145.69±5.0	91.56±4.0	61.04±4.0
8	31.14±4.0	120.1±5.0	310.4±7.0	256.1±9.0	189±5.0	107.4±8.0
24	54.06±5.0	215.31±9.0	514.3±14.0	467.8±16.0	376.4±11.0	197.5±10.0

The steady-state flux (*J*ss) of 6-MNA **(16)**, BPA **(17)** and their salts **(18a-19e)** were given in **Table 3.1.9** All the salts have shown higher flux values than the parent NSAIDs. Amongst all the salts, salts **(18b** and **19b)** have shown highest steady state flux from 6-MNA and BPA series respectively.

Table 3.1.9: Steady state flux of 6-MNA **(16)**, BPA **(17)** and their salts

Derivative	*J*ss (µg/cm^{2}h)	Derivative	*J*ss (µg/cm^{2}h)
16	0.489	**17**	0.42
18a	2.15	**19a**	1.75
18b	4.03	**19b**	4.14
18c	3.13	**19c**	3.76
18d	1.52	**19d**	3.11
18e	1.29	**19e**	1.60

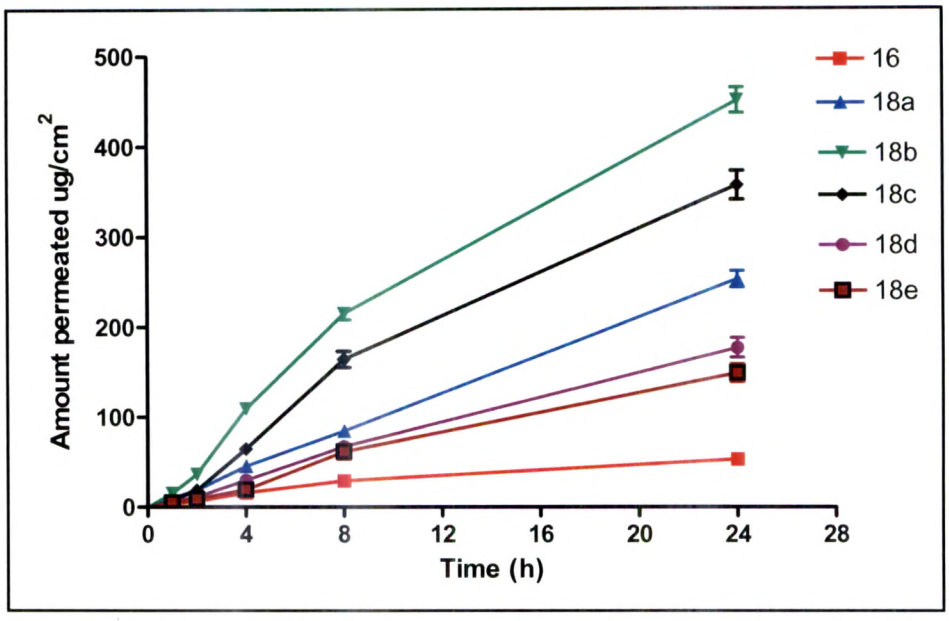

Fig. 3.1.14: Permeation profiles (mean SEM, n=3) for **16** and its salts **(18a-18e)**

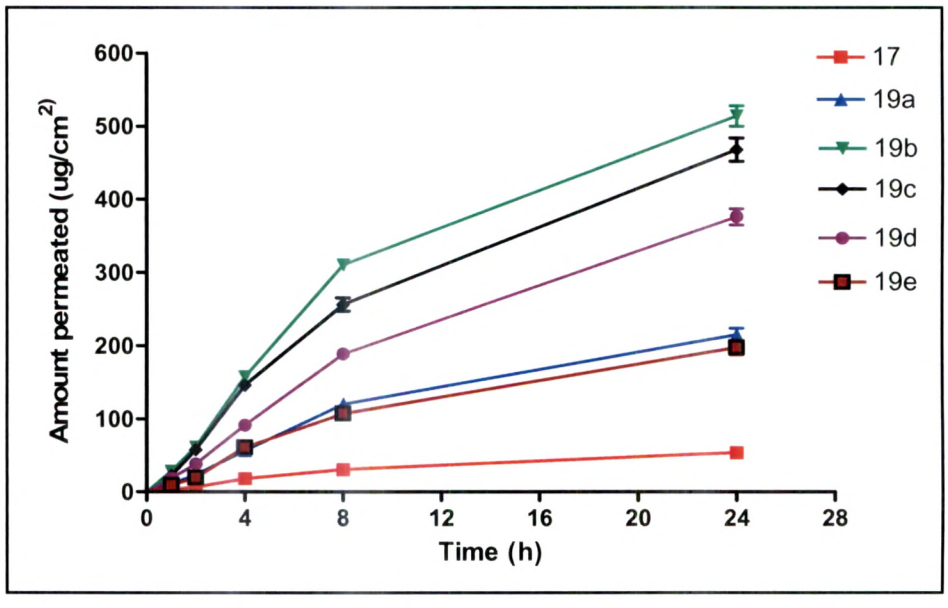

Fig. 3.1.15: Permeation profiles (mean SEM, n=3) for **17** and its salts **(19a-19e)**

The ethanolamine salts **(18b, 19b)** displayed 9-10 times higher flux than the parent NSAIDs. The result also showed that salts with higher flux have a balance between solubility and partition coefficient. Further, except for sodium salt all the salts have lower melting points than the parent drugs and higher permeability through the skin, which support previous, reports[28] indicating that a decrease in melting point or conversion of solid state to liquid state improves the permeability of drugs through skin.

3.2 Prodrug approach

The work carried out towards achieving the proposed plan has been discussed under the following three main headings.

3.2.1. Design of prodrugs

3.2.2. Syntheses and characterization of prodrugs

3.2.3. Physicochemical evaluation of the prodrugs

3.2.3.1. Determination of aqueous solubility

3.2.3.2. Determination of Log *P*

3.2.3.3. Hydrolyses kinetics study

3.2.3.4. *In vitro* skin permeation study

3.2.1 Design of prodrugs

In order to improve the permeability of 6-MNA **(16)** the first essential requirement is to improve the aqueous solubility with balanced log*P*. To achieve this it was planned to synthesize piperazine derivatives of **16** as shown in **Fig. 3.2.1.** The designed prodrug derivatives would contain piperazine ring moiety with various electron withdrawing or electron donating substituents to modify the *p*Ka, suitable linker to impart lipophilicity and hydrolysable ester grouping. Piperazine is freely soluble in water and ethylene glycol. It is a weak base with a pK_b of 4.19; the *p*H of a 10% aqueous solution of piperazine is 10.8-11.8.

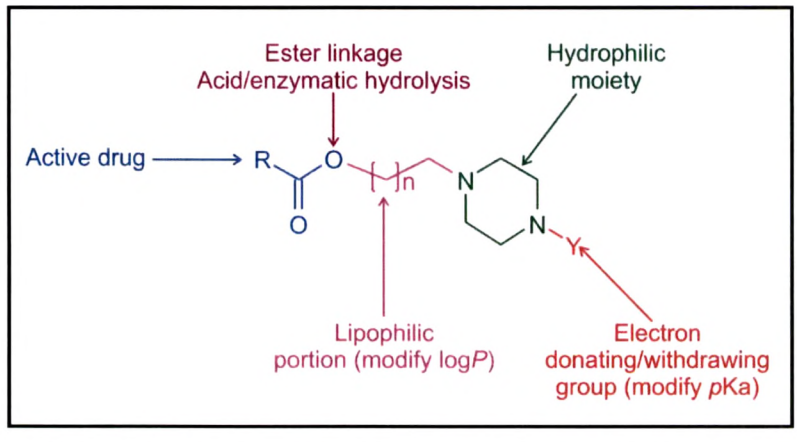

Fig. 3.2.1: General structure of designed prodrugs of 6-MNA **(16)**

In order to know the structural properties of the designed prodrugs at *p*H 5 and 7.4 QikProp 3.2 software was used.[2] QikProp is quick, accurate, easy-to-use software designed by Professor William L. Jorgensen which predicts absorption, distribution, metabolism, and excretion (ADME) parameters. QikProp software predicts physically

significant descriptors and pharmaceutically relevant properties of organic molecules, either individually or in batches. For each successfully processed molecule, QikProp produces the following descriptors and properties.

Table 3.2.1: Various descriptors used in QikProp 3.2 software.

Property or descriptor	Description	Recommended value
MW	Molecular weight of the molecule	130-725
Dipole	Computed dipole moment of the molecule	1.0-12.25
SASA	Total solvent accessible surface area (SASA) in square angstroms using a probe with a 1.4 Å radius	300-1000
FOSA	Hydrophobic component of the SASA (saturated carbon and attached-H).	0-750
FISA	Hydrophilic component of the SASA (SASA on N, O, and H on heteroatoms)	7-330
PISA	∏ (Carbon and attached hydrogen) component of the SASA.	0-450
QPlogPo/w	Predicted octanol/water partition coefficient	-2.0-6.5
QPlogS	Predicted aqueous solubility, log S. S in mol dm^{-3} concentration of the solute in a saturated solution that is in equilibrium with the crystalline solid.	-6.5-0.5
QPlogKp	Predicted skin permeability, log *Kp*.	-8.0- -1.0)
QPlogKhsa	Prediction of binding to human serum albumin.	-1.5-1.5

The molecules were built within Maestro using the build module and prepared for analysis by using LigPrep module at physiological *p*H of Schrödinger 2009 by keeping all other parameters to their standard values. Structural properties were calculated by using QikProp as given in **Table 3.2.4-3.2.5.** *p*Ka values for structures were calculated using Epik at physiological *p*H 7.4 using H_2O solvent.[3] The obtained results are given in **Table 3.2.6.**

Table 3.2.2: Various protonated forms obtained for tweleve derivatives at *p*H 5.0

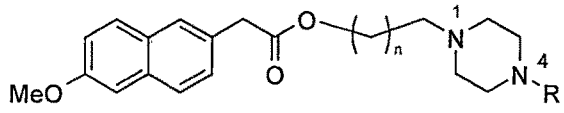

Entry ID	n	R	Protonation of Nitrogen at *p*H 5	
			N^1	N^4
TD1	1	$-CH_3$	+	+
TD2	1	$-CH_2CH_3$	+	+
TD3	1	$-COCH_3$	+	--
TD4	1	-Ph	+	--
TD4A	1	-Ph	+	+
TD5	1	$-CH_2CH_2CH_3$	+	+
TD6	1	$-CH_2CH_2CH_2CH_3$	+	+
TD7	2	$-CH_3$	+	+
TD8	2	$-CH_2CH_3$	+	+
TD9	2	$-COCH_3$	+	--
TD10	2	-Ph	+	+
TD10A	2	-Ph	+	--
TD11	2	$-CH_2CH_2CH_3$	+	+
TD12	2	$-CH_2CH_2CH_2CH_3$	+	+

+ = Protonated, -- = Not protonated

Table 3.2.3: Various protonated forms obtained for twelve derivatives at *p*H 7.4

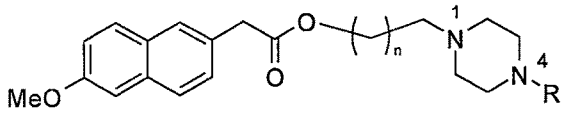

Entry ID	n	R	Protonation of Nitrogen at *p*H 5	
			N^1	N^4
TD1	1	$-CH_3$	--	--
TD1A	1	$-CH_3$	+	--
TD1B	1	$-CH_3$	--	+
TD1C	1	$-CH_3$	+	+
TD2	1	$-CH_2CH_3$	--	--
TD2A	1	$-CH_2CH_3$	+	--
TD2B	1	$-CH_2CH_3$	--	+
TD2C	1	$-CH_2CH_3$	+	+
TD3	1	$-COCH_3$	+	--
TD4	1	-Ph	+	--
TD5	1	$-CH_2CH_2CH_3$	--	--
TD5A	1	$-CH_2CH_2CH_3$	+	--
TD5B	1	$-CH_2CH_2CH_3$	--	+
TD5C	1	$-CH_2CH_2CH_3$	+	+
TD6	1	$-CH_2CH_2CH_2CH_3$	--	--
TD6A	1	$-CH_2CH_2CH_2CH_3$	+	--
TD6B	1	$-CH_2CH_2CH_2CH_3$	--	+
TD6C	1	$-CH_2CH_2CH_2CH_3$	+	+
TD7	2	$-CH_3$	--	--
TD7A	2	$-CH_3$	+	--
TD7B	2	$-CH_3$	--	+
TD7C	2	$-CH_3$	+	+
TD8	2	$-CH_2CH_3$	--	--
TD8A	2	$-CH_2CH_3$	+	--
TD8B	2	$-CH_2CH_3$	--	+
TD8C	2	$-CH_2CH_3$	+	+
TD9	2	$-COCH_3$	+	--
TD10	2	-Ph	+	--
TD11	2	$-CH_2CH_2CH_3$	--	--
TD11A	2	$-CH_2CH_2CH_3$	+	--
TD11B	2	$-CH_2CH_2CH_3$	--	+
TD11C	2	$-CH_2CH_2CH_3$	+	+
TD12	2	$-CH_2CH_2CH_2CH_3$	--	--
TD12A	2	$-CH_2CH_2CH_2CH_3$	+	--
TD12B	2	$-CH_2CH_2CH_2CH_3$	--	+
TD12C	2	$-CH_2CH_2CH_2CH_3$	+	+

+ = Protonated, -- = Not protonated

Table 3.2.4: Design parameters and structural properties of various protonated forms at *p*H 5.0

Entry ID	MW	Dipole	SASA	FOSA	FISA	PISA	QPlogPo/w	QPlogS	QPlogKp	QPlogKhsa
MNA	216.236	4.352	444.137	136.445	100.097	207.596	3.212	-3.832	-2.345	-0.191
TD1	342.437	3.885	674.199	432.612	36.132	205.454	2.694	-2.043	-5.011	0.006
TD2	356.464	3.803	703.38	463.954	33.96	205.466	3.068	-2.433	-4.875	0.123
TD3	370.447	6.281	697.287	419.979	71.832	205.476	2.23	-2.023	-3.606	-0.419
TD4	404.508	4.647	753.889	338.856	23.969	391.063	5.104	-5.296	-2.07	0.761
TD4A	404.508	3.567	764.033	341.77	30.995	391.268	5.126	-5.489	-2.199	0.792
TD5	370.491	3.774	736.49	497.364	33.673	205.453	3.466	-2.898	-4.773	0.257
TD6	384.517	3.767	769.175	530.063	33.657	205.455	3.86	-3.355	-4.677	0.39
TD7	356.464	3.428	720.827	462.441	52.747	205.639	3.045	-2.764	-5.22	0.171
TD8	370.491	2.112	764.115	499.389	57.084	207.642	3.454	-3.421	-5.197	0.323
TD9	384.474	5.784	751.772	451.368	94.771	205.634	2.565	-2.895	-3.932	-0.242
TD10	418.535	4.397	807.847	369.905	46.609	391.333	5.441	-6.156	-2.39	0.937
TD10A	418.535	3.238	807.484	371.096	45.007	391.381	5.494	-6.149	-2.361	0.956
TD11	384.517	3.371	783.035	526.995	50.403	205.637	3.818	-3.617	-4.985	0.423
TD12	398.544	3.365	815.766	559.76	50.373	205.634	4.212	-4.075	-4.889	0.555

Table 3.2.5: Design parameters of various protonated forms at *p*H 7.4

Entry ID	MW	Dipole	SASA	FOSA	FISA	PISA	QPlogPo/w	QPlogS	QPlogKp	QPlogKhsa
MNA	216.236	4.352	444.137	136.445	100.097	207.596	3.212	-3.832	-2.345	-0.191
TD1	342.437	3.592	685.361	427.866	51.84	205.656	2.621	-2.255	-5.3	0.022
TD1A	342.437	3.293	665.391	419.957	39.965	205.469	2.566	-1.876	-5.081	-0.039
TD1B	342.437	3.511	685.503	429.624	50.219	205.66	2.636	-2.257	-5.27	0.024
TD1C	342.437	3.885	674.199	432.612	36.132	205.454	2.694	-2.043	-5.011	0.006
TD2	356.464	3.504	716.004	461.585	48.764	205.655	3.016	-2.673	-5.147	0.146
TD2A	356.464	3.25	694.709	452.651	36.577	205.48	2.953	-2.269	-4.923	0.08
TD2B	356.464	3.436	714.667	462.323	46.684	205.66	3.033	-2.647	-5.109	0.147
TD2C	356.464	3.803	703.38	463.954	33.96	205.466	3.068	-2.433	-4.875	0.123
TD3	370.447	6.281	697.287	419.979	71.832	205.476	2.23	-2.023	-3.606	-0.419
TD4	404.508	4.647	753.889	338.856	23.969	391.063	5.104	-5.296	-2.07	0.761
TD5	370.491	3.469	748.968	494.501	48.812	205.655	3.411	-3.134	-5.052	0.279
TD5A	370.491	3.252	727.377	485.437	36.462	205.478	3.347	-2.725	-4.825	0.213
TD5B	370.491	3.409	747.891	495.741	46.492	205.658	3.428	-3.114	-5.009	0.279
TD5C	370.491	3.774	736.49	497.364	33.673	205.453	3.466	-2.898	-4.773	0.257
TD6	384.517	3.46	781.854	527.402	48.798	205.654	3.805	-3.595	-4.956	0.412
TD6A	384.517	3.244	760.269	518.393	36.416	205.461	3.743	-3.186	-4.728	0.346
TD6B	384.517	3.404	780.518	528.383	46.478	205.657	3.821	-3.57	-4.913	0.412

TD6C	384.517	3.767	769.175	530.063	33.657	205.455	3.86	-3.355	-4.677	0.39
TD7	356.464	3.481	720.644	461.057	53.952	205.636	3.009	-2.761	-5.243	0.159
TD7A	356.464	3.614	710.961	447.778	57.542	205.64	2.905	-2.577	-5.309	0.123
TD7B	356.464	2.915	731.703	465.735	58.326	207.641	3.059	-2.97	-5.316	0.193
TD7C	356.464	3.428	720.827	462.441	52.747	205.639	3.045	-2.764	-5.22	0.171
TD8	370.491	3.029	764.472	500.012	56.81	207.65	3.438	-3.428	-5.192	0.315
TD8A	370.491	3.546	740.351	480.748	53.962	205.641	3.295	-2.971	-5.147	0.243
TD8B	370.491	2.958	760.903	498.462	54.79	207.65	3.456	-3.361	-5.155	0.317
TD8C	370.491	2.112	764.115	499.389	57.084	207.642	3.454	-3.421	-5.197	0.323
TD9	384.474	5.784	751.772	451.368	94.771	205.634	2.565	-2.895	-3.932	-0.242
TD10	418.535	4.397	807.847	369.905	46.609	391.333	5.441	-6.156	-2.39	0.937
TD11	384.517	3.043	797.314	532.949	56.717	207.648	3.833	-3.888	-5.094	0.448
TD11A	384.517	3.519	772.451	512.966	53.855	205.629	3.685	-3.417	-5.049	0.374
TD11B	384.517	2.949	794.134	531.885	54.605	207.645	3.851	-3.828	-5.056	0.449
TD11C	384.517	3.371	783.035	526.995	50.403	205.637	3.818	-3.617	-4.985	0.423
TD12	398.544	3.048	830.194	565.846	56.697	207.652	4.227	-4.348	-4.998	0.581
TD12A	398.544	3.515	805.395	545.934	53.841	205.62	4.08	-3.878	-4.953	0.507
TD12B	398.544	2.957	826.759	564.526	54.589	207.644	4.244	-4.283	-4.959	0.582
TD12C	398.544	3.365	815.766	559.76	50.373	205.634	4.212	-4.075	-4.889	0.555

Table 3.2.6: *p*Ka of 6-MNA **(16)** and its derivatives at physiological *p*H 7.4 using H_2O as solvent.

Title	pKa 1	pKa 2
MNA	4.316	-
TD1	3.572	7.719
TD2	3.657	7.863
TD3	6.335	-
TD4	3.49	7.324
TD5	3.675	7.892
TD6	3.678	8.079
TD7	4.214	7.749
TD8	4.299	7.893
TD9	6.592	-
TD10	3.681	7.581
TD11	4.317	7.922
TD12	4.32	8.109

3.2.2 Syntheses and characterization of prodrugs (25a-25d and 26a-26d)

Considering the optimum values for ideal prodrug design from the above studies and feasibility of their synthesis it was planned to synthesize eight derivatives **(25a-25d** and **26a-26d)** as shown below. **Scheme-1** was employed to synthesize piperazinylalkyl ester prodrugs of 6-MNA **(16)**.

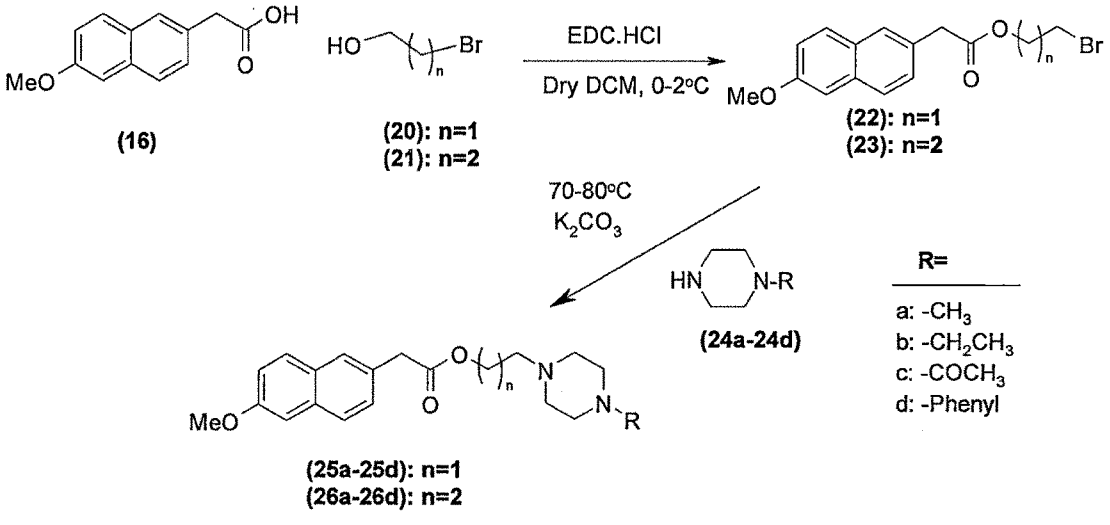

Scheme-1: Synthesis of prodrugs of 6-MNA **(16)**

6-MNA **(16)** was coupled with 2-bromoethanol **(20)** using 1-ethyl-3-(3-dimethylaminopropyl)carbodiimide (EDC) as coupling agent and dimethylaminopyridine (DMAP) as catalyst in dry dichloromethane (DCM) at 0-2 ^{0}C to obtain the desired intermediate 2-bromoethyl 2-(6-methoxy-2-naphthyl)acetate **(22).**

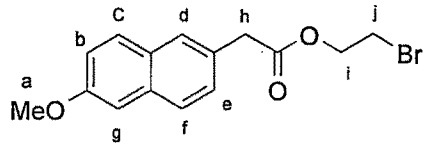

(22)

The structure was confirmed by IR spectroscopy which showed strong absorption peak at 1727 cm^{-1} due to carbonyl stretching of ester group. PMR spectrum showed multiplet at δ 7.71-7.11 of six naphthalene protons (Ar-$H_{b\text{-}g}$), a triplet at δ 4.42-4.39 due to methylene protons (-CH_{2i}) with coupling constant equal to 6.08 Hz. Methoxy protons (-OC$H_{3/a}$) appeared at δ 3.91 as singlet and methylene protons attached to aromatic ring (-CH_{2h}) appeared at δ 3.79. A triplet due to methylene protons (-C$H_{2/j}$) was observed at δ 3.51-3.48 with coupling constant equal to 6.08 Hz.

Similarly another intermediate **(23)** required for synthesis of the final derivatives was prepared according to the same procedure as adopted for **22** using 6-MNA **(16)** and 3-bromo-1-propanol **(21)** to give 3-bromopropyl 2-(6-methoxy-2-naphthyl)acetate **(23)** as a white solid.

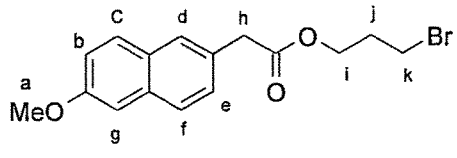

(23)

It was confirmed by IR spectroscopy which showed strong absorption peak at 1735 cm^{-1} due to carbonyl stretching of ester group. The PMR spectrum of compound **(23)** showed multiplet at δ 7.71-7.11 for the six naphthalene protons (Ar-$H_{b\text{-}g}$) and methylene protons (-C$H_{2/i,}$) appeared at δ 4.25-4.22 as a triplet with coupling constant equal to 6.4 Hz. Methoxy protons (-OC$H_{3/a}$) showed singlet at δ 3.91 and a singlet of methylene protons attached to aromatic ring (Ar-C$H_{2/h}$) appeared at δ 3.75. Other methylene protons (-C$H_{2/k}$) appeared at δ 3.40-3.36 as a triplet with coupling constant equal to 6.04 Hz. Multiplet at δ 2.18-2.11 appeared due to methylene protons (-C$H_{2/j}$) with coupling constant equal to J=6.0 Hz.

3.2.2.1 Syntheses of substituted piperazinethyl esters (25a-25d) of 6-MNA (16)

Synthesis of substituted piperazinethyl esters **(25a-25d)** of 6-MNA **(16)** were carried out by using synthetic route shown in **Scheme-1**. The reaction of 2-bromoethyl 2-(6-methoxy-2-naphthyl)acetate **(22)** with substituted piperazines **(24a-24d)** was accomplished by refluxing the reagents in dry acetone with two drops of DMF and potassium carbonate at 70-80 ^{0}C till the reaction got completed.

The synthesis of 2-(4-methylpiperazin-1-yl)ethyl 2-(6-methoxy-2-naphthyl)acetate **(25a)** was carried out in the same fashion as described above by reacting 2-bromoethyl 2-(6-methoxy-2-naphthyl)acetate **(22)** and *N*-methylpiperazine **(24a)** to get brown oily product **(25a)**.

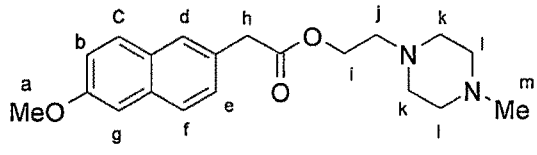

(25a)

The IR spectrum **(Fig. 3.2.2.A)** of the ester **(25a)** showed absorption peak at 1730 cm^{-1} due to carbonyl stretching of ester group. The peaks at 1264 cm^{-1} and 1148 cm^{-1} are due to C-O and C-N stretching vibration's respectively. Its PMR spectrum **(Fig. 3.2.2.B)** showed multiplet at δ 7.63-7.03 for six naphthalene protons (Ar-$H_{b\text{-}g}$) and a triplet at δ 4.16-4.13 due to methylene (-C$H_{2/i}$) protons with coupling constant equal to 5.8 Hz. A singlet due to methoxy protons (-C$H_{3/a}$) appeared at δ 3.83 and of methylene (Ar-C$H_{2/h}$) at δ 3.68. The other methylene protons (N-C$H_{2/j}$) showed triplet at δ 2.54-2.51 with coupling constant equal to 5.8 Hz. The piperazine protons appeared as multiplet at δ 2.38-2.27 (-$H_{k,l}$) and *N*-methyl protons (-C$H_{3/m}$) at δ 2.16 as a singlet.

^{13}C-NMR spectrum **(Fig. 3.2.2.C)** shows peak at 171.67 for carbonyl carbon. Aromatic carbons of naphthalene ring (10C) appear in the range of δ 157.62-105.56. Methoxy carbon appears at δ 56.2 and -OCH_2 at δ 62.31. Four piperazine carbons were observed at δ 52.12-55.3. Other aliphatic carbons appeared at δ 52.93 (N-CH_2), δ 52.12-52.64 (2C, piperazine, *C*-2,6), δ 45.70 (Ar-CH_2-) and δ 41.20 (1C, N-CH_3). Mass spectrum **(Fig. 3.2.2.D)** shows molecular ion peak at 342.5 (M^+) and also M+2 peak at 344.0 which is base peak. The compound showed high chromatographic purity (>98.2 %) by HPLC **(Fig. 3.2.2.E)**.

Other compounds **(25b-25d)** of the series were prepared in the same fashion as described for derivative **(25a)**; their analytical data are given in **Table 3.2.7.**

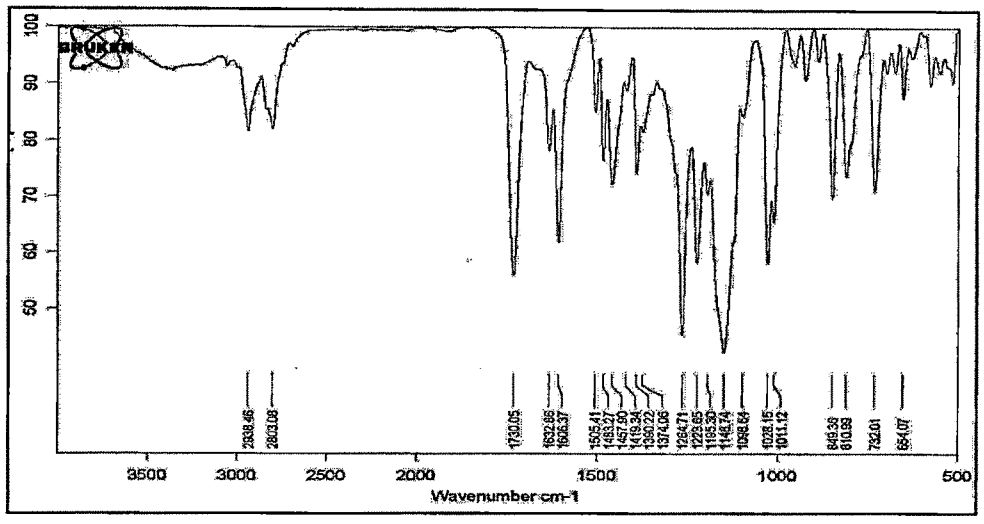
BRUKER
100
90
80
70
60
50
2938.46
2803.08
1730.05
1632.86
1605.37
1505.41
1483.27
1457.90
1419.34
1390.22
1374.06
1284.71
1225.85
1165.33
1145.74
1098.64
1028.15
1011.12
849.38
810.98
752.01
664.07
3500
3000
2500
2000
1500
1000
500
Wavenumber cm-1

(A)

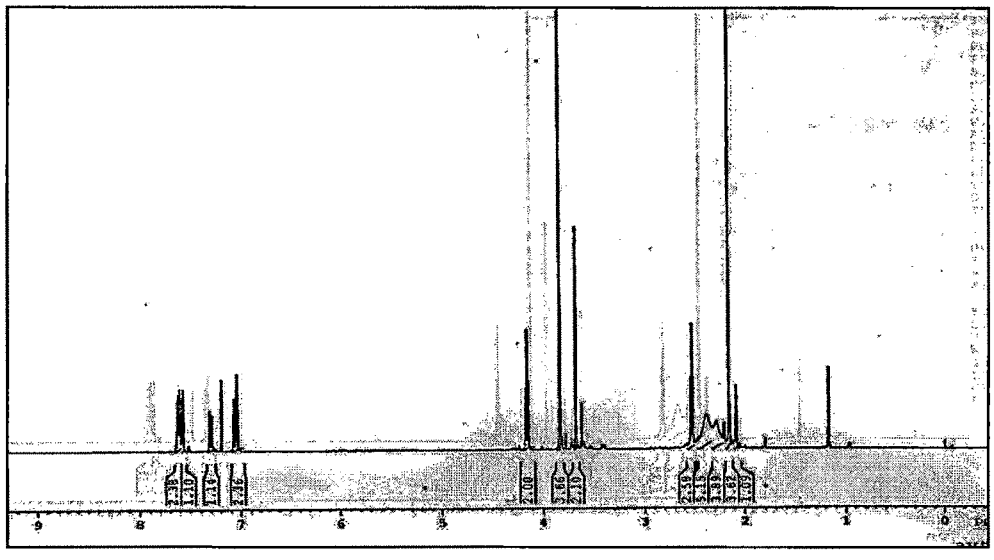

(B)

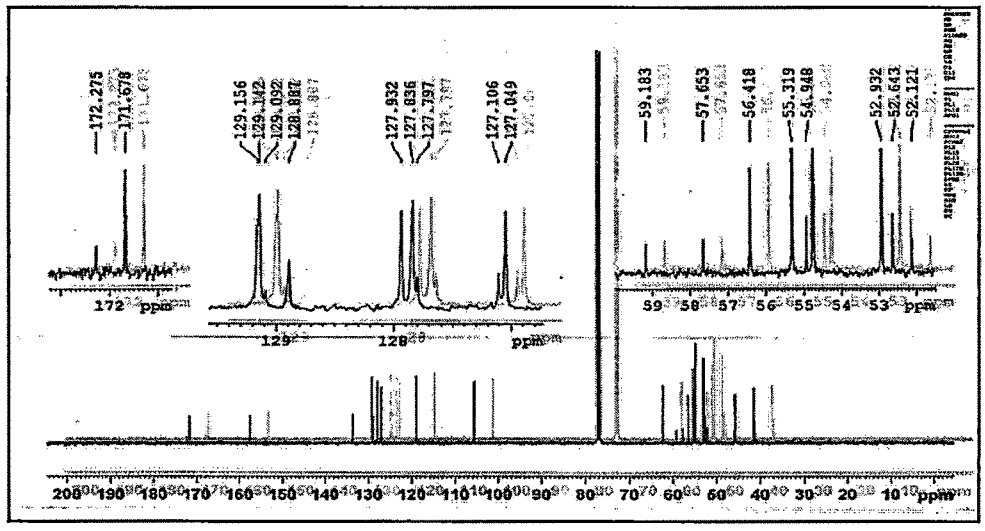
172.275
171.678
129.156
129.142
129.092
127.932
127.836
127.797
127.106
127.049
59.183
57.653
56.418
55.319
54.948
52.932
52.643
52.121
172 ppm
129
128
ppm
59
58
57
56
55
54
53 ppm
ppm

(C)

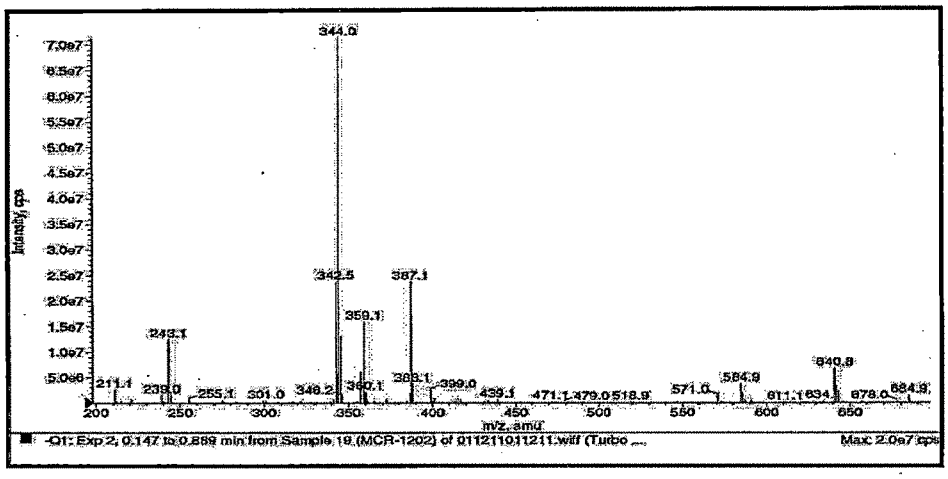

(D)

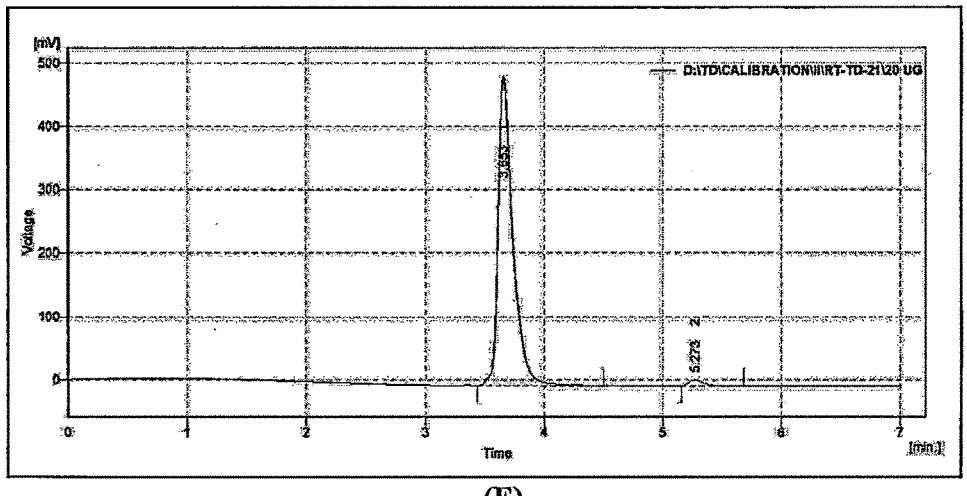

(E)

Fig. 3.2.2: Spectra of derivative **(25a)**; IR spectrum **(A)**, ^{1}H-NMR **(B)**, ^{13}C-NMR **(C)**, Mass spectrum **(D)** and HPLC chromatogram **(E)**.

3.2.2.2 Synthesis of substituted piperazinpropyl esters (26a-26d) of 6-MNA

Synthesis of substituted piperazinylalkyl esters **(26a-26d)** of 6-MNA were carried out as per the synthetic route shown in **Scheme-1**. The reaction of 3-bromopropyl 2-(6-methoxy-2-naphthyl)acetate **(23)** with substituted piperazines **(24a-24d)** was accomplished by refluxing both the reactants in dry acetone with two drops of DMF and potassium carbonate at 70-80 ^{0}C till the reaction got completed.

The product was isolated and purified by column chromatography to get a brown oily product. IR spectrum **(Fig. 3.2.3. A)** of the compound **(26a)** showed a strong absorption peak at 1732 cm^{-1} due to carbonyl stretching of ester group. The peaks at 1398 cm^{-1} and 1163 cm^{-1} are due to C-O and C-N stretching vibrations respectively. The PMR signals of compound **(26a)** appeared at δ 7.62-7.02 (m, 6H, Ar-*H*b-g), 4.07-4.04 (t, 2H, -

$CH_{2/i}$), 3.81 (s, 3H, -OC$H_{3/a}$), 3.64 (s, 2H, Ar-C$H_{2/h}$), 2.34-2.28 (m, 8H, N-C$H_{2/l\text{-}m}$), 2.27-2.23 (t, 2H, -C$H_{2/k}$), 2.16 (s, 3H, -C$H_{3/n}$) and 1.75-1.74 (m, 2H, -C$H_{2/j}$) **(Fig. 3.2.3. B)**

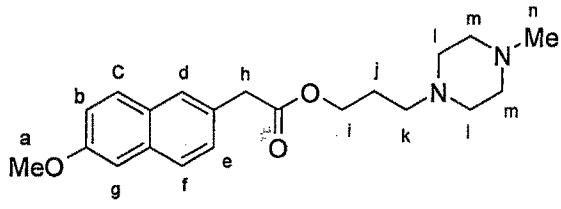

(26a)

^{13}C-NMR spectrum **(Fig. 3.2.3. C)** shows peaks at 17.76, 168.92, 157.65, 133.59-105.56, 62.94, and 55.32-21.31. The mass spectrum **(Fig. 3.2.3. D)** of compound **(26a)** shows peak at 356.03 (M^+) which is also the base peak. The compound also showed high chromatographic purity (>98 %) by HPLC.

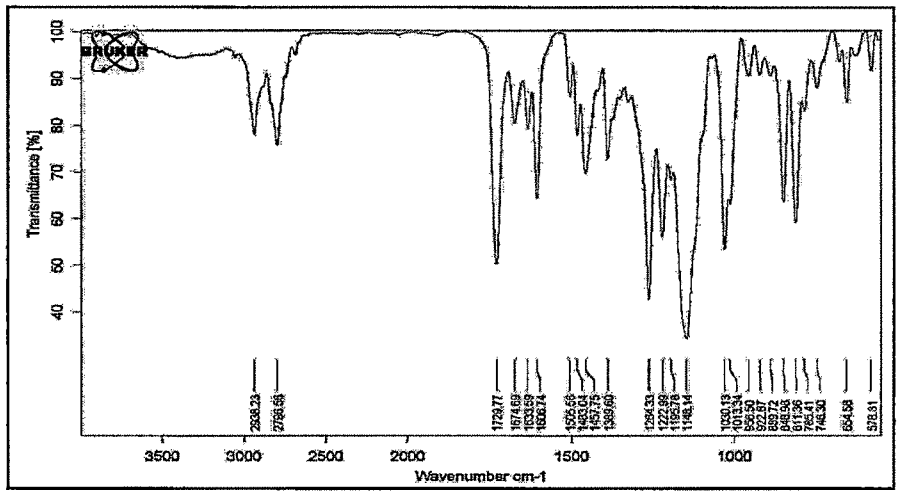

(A)

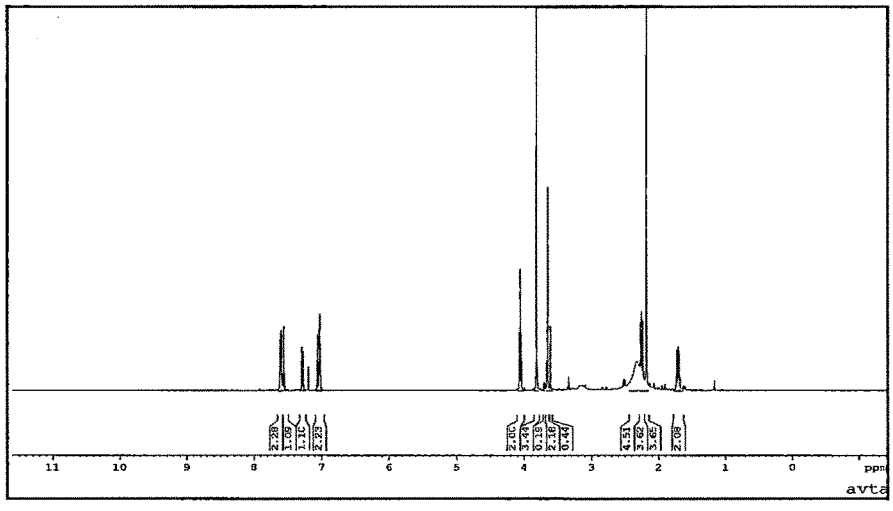

(B)

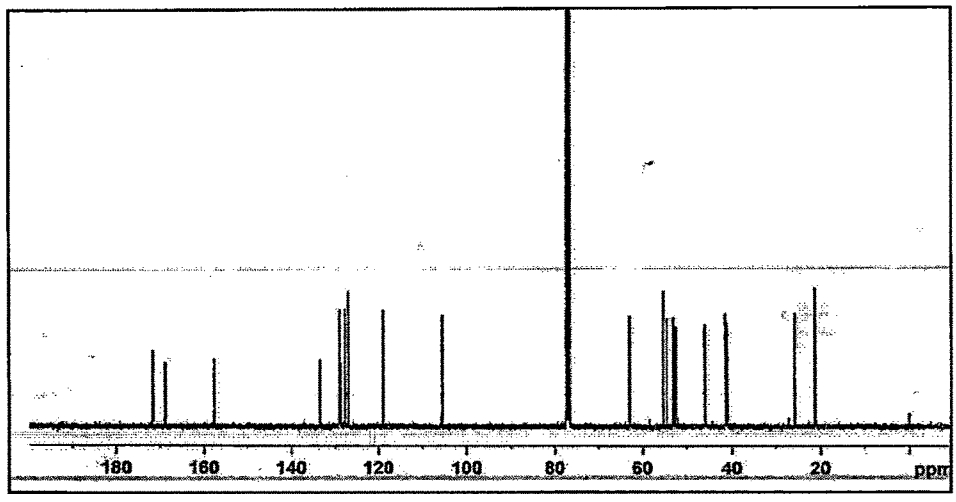

(C)

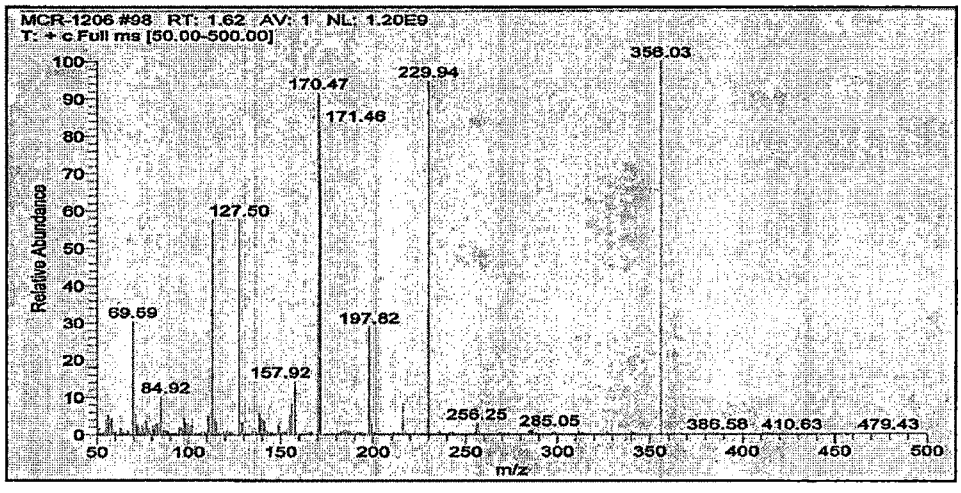

(D)

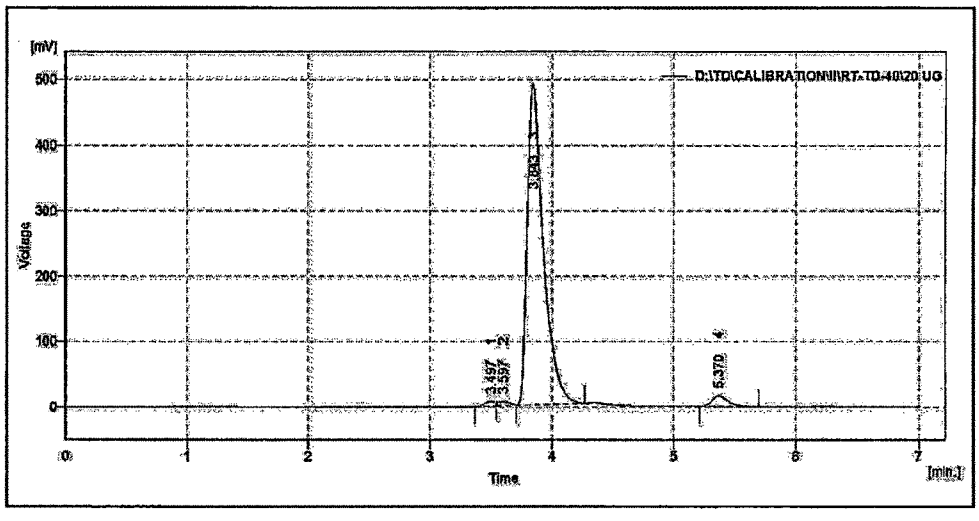

(E)

Fig. 3.2.3: Spectra of derivative **(26a)**; IR spectrum **(A)**, ^{1}H-NMR **(B)**, ^{13}C-NMR **(C)**, Mass spectrum **(D)** and HPLC chromatogram **(E)**.

Syntheses of other derivatives **(26b-26d)** from this series were carried out by the procedure as described above and their spectral data is given in **Table 3.2.7**

Table 3.2.7: Spectral data of derivatives **(25b-25d** and **26b-26d)**

Compound No.	IR Peaks (cm^{-1})	PMR Peaks (δ)
25b	1731, 1264,1151	7.03-7.63 (m, 6H), 4.14-4.17 (t, 2H), 3.83 (s, 3H), 3.68 (s, 2H), 2.52-2.54 (t, 2H), 2.34-2.38 (m, 8H), 2.26-2.31 (q, 2H), 0.95-0.99 (t, 3H)
25c	1730, 1263, 1150	7.03-7.63 (m, 6H), 4.13-4.16 (t, 2H), 3.82 (s, 3H), 3.67 (s, 2H), 3.40-3.43 (t, 2H), 3.11-3.13 (t, 2H), 2.50-2.52 (t, 2H), 2.27-2.29 (t, 2H), 2.19-2.21 (t, 2H), 1.90 (s, 3H)
25d	1720, 1234, 1147	7.22-7.70 (m, 6H), 6.80-7.15 (m, 5H), 4.27-4.29 (t, 2H), 3.90 (s, 3H), 3.77 (s, 2H), 2.95-3.02 (t, 4H), 2.64-2.67 (t, 2H), 2.49-2.52 (t, 4H)
26b	1732, 1265,1156	6.95-7.55 (m, 6H), 3.96-3.99 (t, 2H), 3.75 (s, 3H), 3.54 (s, 2H), 2.47-2.50 (t, 2H), 2.26-2.42 (m, 8H), 2.19-2.21 (m, 2H), 1.55-1.58 (m, 2H), 0.94-0.97 (m, 3H)
26c	1728, 1263, 1150	7.11-7.70 (m, 6H), 4.13-4.17 (t, 2H), 3.91 (s, 3H) 3.73 (s, 2H), 3.54-3.57 (t, 2H), 3.35-3.38 (t, 2H), 2.27-2.33 (m, 6H), 2.05 (s, 3H), 1.77-1.80 (m, 2H)
26d	1736, 1267, 1155.	7.15-7.63 (m, 6H), 6.75-7.07 (m, 5H), 4.07-4.11 (t, 2H), 3.81 (s, 3H), 3.66 (s, 2H), 3.04-3.06 (t, 4H), 2.40-2.43 (t, 4H), 2.28-2.32 (t, 2H), 1.73-1.77 (m, 2H)

3.2.3 Physicochemical evaluation of 6-MNA and the synthesized prodrugs (25a-25d and 26a-26d)

For the evaluation of various physicochemical parameters such as aqueous solubility, partition coefficient and hydrolysis kinetics study, HPLC method has been developed. Calibration curve for 6-MNA **(16)** and its different prodrugs were plotted and their linearity calculated.

Chromatographic conditions

Chromatography was performed under isocratic conditions at a flow-rate of 0.9 ml/min. The mobile phase consisted of phosphate buffer (PB, 15 mM): acetonitrile (1:1)

and methanol:acetonitrile (9:1). Solution of the prodrug was filtered through Whatman filter paper (0.2 μ) and degassed for 10 min in an ultrasonic bath. An aliquot of sample solution (20 μl) was injected onto the analytical column with a manual injection, the column effluent was monitored at 227 nm.

Table 3.2.8: Chromatographic conditions for **(16)** and derivatives **(25a-26d)**

Derivative	Linearity range (μg)	Mobile phase composition	Flow rate (ml/min.)	Retention time (R_t Min.)	λ_{max}
16	0.5-40	PB:ACN (1:1)	0.9	4.73 ± 0.2	230
25a				3.65 ± 0.2	227
25b				3.88 ± 0.2	
26a				3.84 ± 0.2	
26b				4.14 ± 0.2	
25c	0.5-30	MeOH:ACN (9:1)	1.0	3.17 ± 0.2	
25d				3.69 ± 0.2	
26c	0.5-45			3.15 ± 0.2	
26d				3.60 ± 0.2	

PB=Phosphate buffer (15 mM), MeOH=Methanol, ACN=Acetonitrile

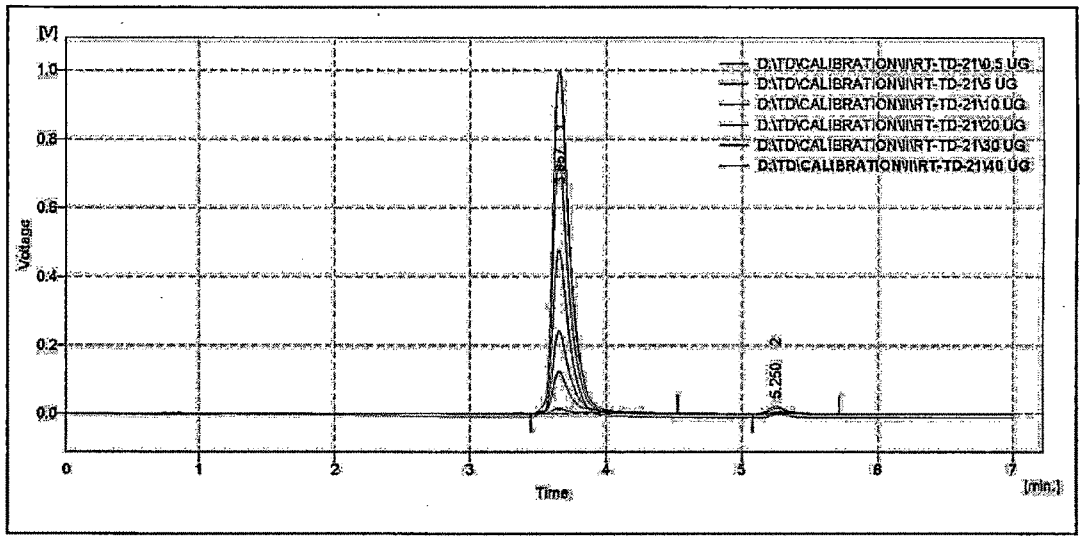

Fig. 3.2.12: Retention time and linearity plot for prodrug **(25a)**

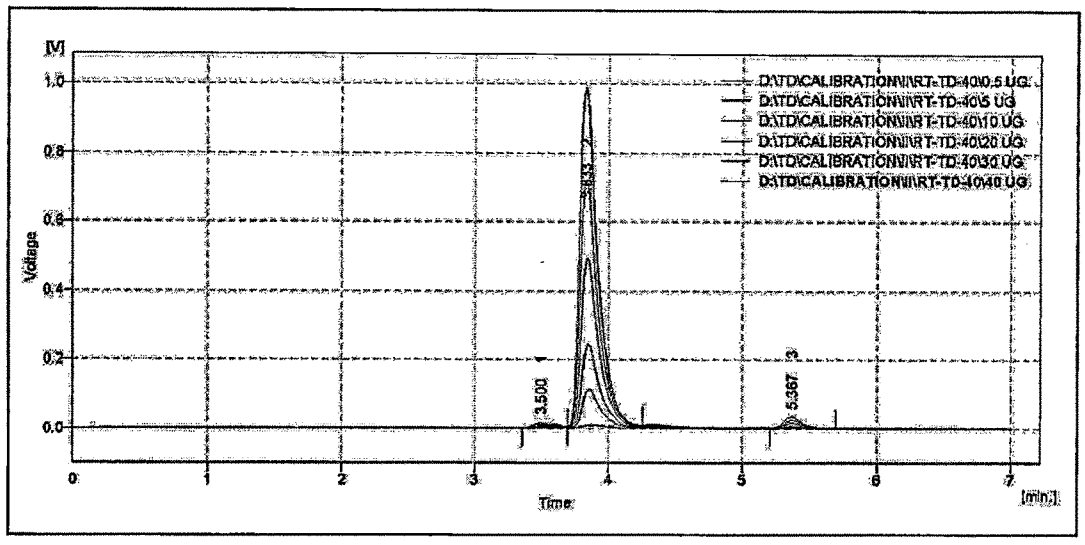

Fig. 3.2.13: Retention time and linearity plot for prodrug **(26a)**

Table 3.2.9: Data for preparation of calibration curve for estimation of **(25a-25b** and **26a-26b)**

Conc. (µg/ml)	Area (mVs) for 25a-25b	Area (mVs) for 26a-26b
0.5	257±5	128±6
5	1209±11	1120±10
10	2166±19	2233±18
20	4224±28	4479±34
30	6410±35	6720±55
40	8735±5	9027±64

Table 3.2.10: Data for preparation of calibration curve for estimation of **(25c-25d and 26c-26d)**

Conc. (µg/ml)	Area (mVs) for 25c-25d	Area (mVs) for 26c-26d
0.5	118 ±8.0	124±9
5	915 ±15.0	1266±15
10	1712±23.0	2712±28
15	2398±36	--
20	3184±45	5720±39
25	4038±67	--
30	4884±74	8615±57
45	--	12450±84

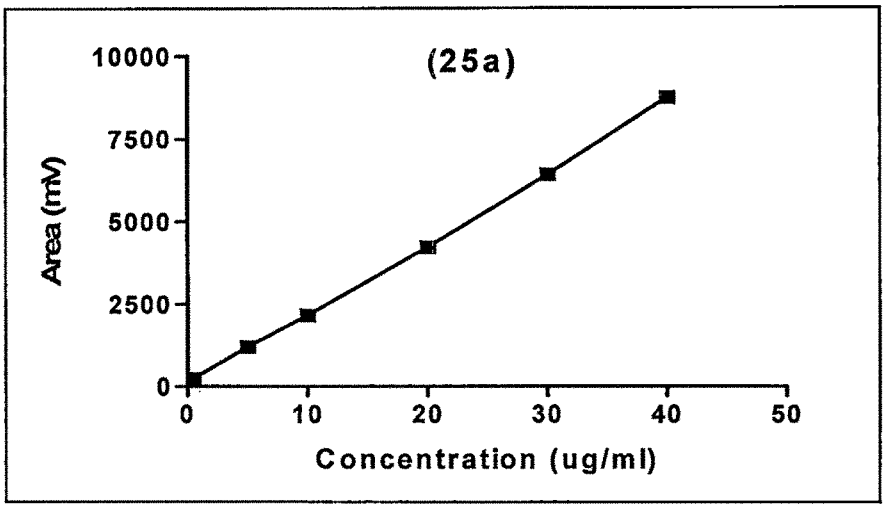

(A): y=216.1x+83.36 (R^2=0.999)

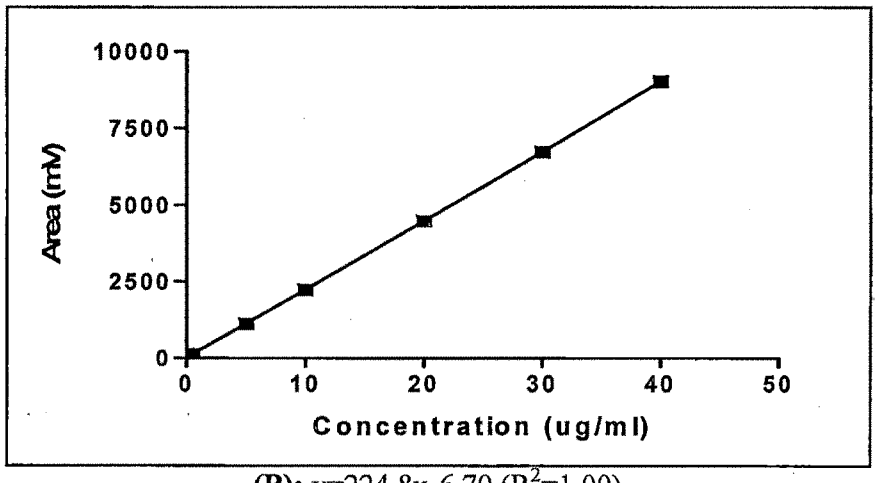

(B): y=224.8x-6.70 (R^2=1.00)

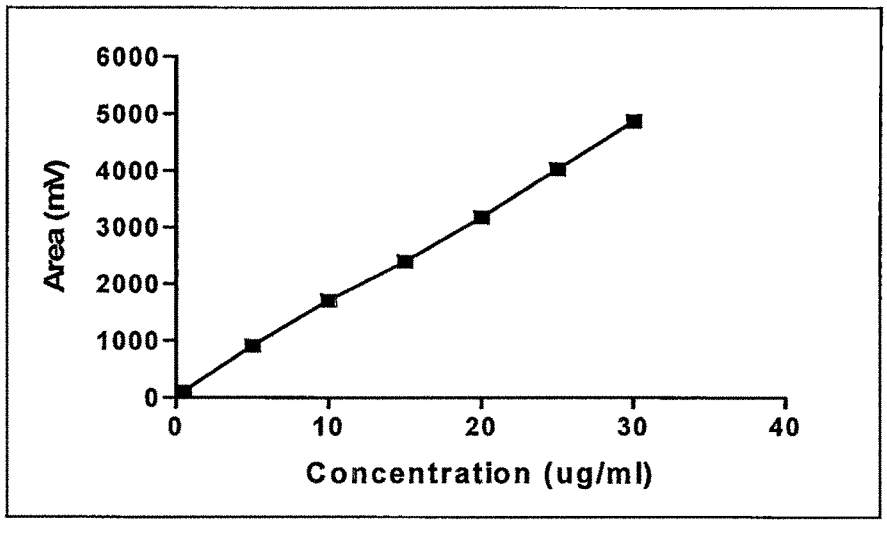

(C): y=162.1x-68.71 (R^2=0.998)

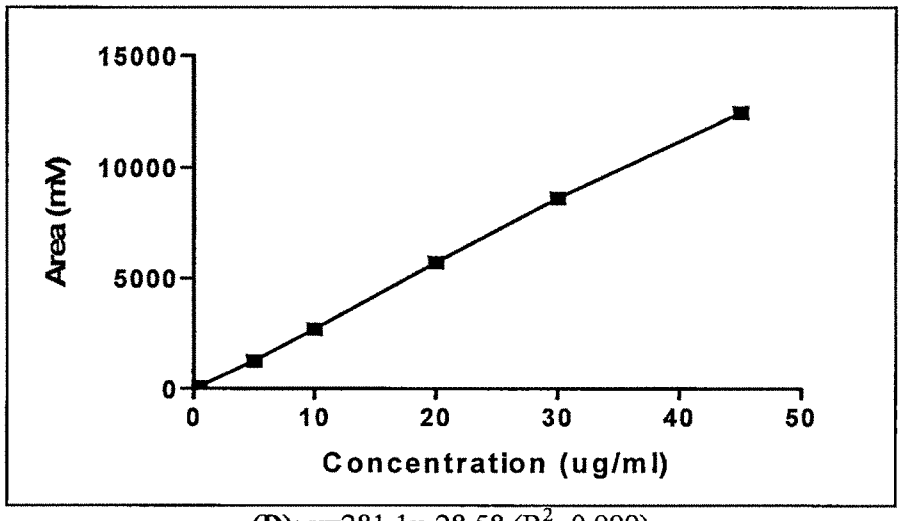

(D): y=281.1x-28.58 (R^2=0.999)

Fig. 3.2.17: Calibration plot for estimation of **A:** 25a-25b; **B:** 26a-26b; **C:** 25c-25d; **D:** 26c-26d

3.2.2.1 Determination of aqueous solubility of the prodrugs

Due to biphasic nature of skin, the ideal topical prodrug should exhibit adequate lipid solubility as well as aqueous solubility. Aqueous solubility of 6-MNA and its prodrugs were determined at the physiological *p*H 7.4 and at *p*H 5.0 the *p*H of of the outer surface of the skin (*p*H 4.2-6.5).[4]

Table 3.2.11: Aqueous solubility of 6-MNA and prodrugs at *p*H 5.0 and *p*H 7.4

Compound	Aqueous Solubility (m*M*)	
	***p*H 5.0**	***p*H 7.4**
16	0.78 ± 0.18	63.34 ± 0.24
25a	23.41 ± 0.16	21.58 ± 0.23
25b	26.01 ± 0.23	12.10 ± 0.17
25c	1.22 ± 0.01	1.49 ± 0.01
25d	0.292 ± 0.002	0.314 ± 0.002
26a	28.41 ± 0.19	20.09 ± 0.16
26b	16.30 ± 0.14	6.20 ± 0.03
26c	6.07 ± 0.02	3.11 ± 0.01
26d	0.267 ± 0.001	0.019 ± 0.0002

Generally an ionized molecule is more water soluble than its unionized form. Because of the acidic character of 6-MNA (*p*Ka 4.16) it is more soluble in aqueous

medium at *p*H 7.4 than at pH 5.0. On the other hand piperazinyl prodrugs **(25a-25b** and **26a-26b)** which possess basic ionizable group (N^1 and/or N^4) get more ionized at *p*H 5.0 than at *p*H 7.4. Piperazinyl prodrugs **(25c-25d** and **26c-26d)** with electron withdrawing groups at N^4 have only one basic ionizable group that makes them less soluble at *p*H 5.0 with no significant differences observed at *p*H 7.4. The aqueous solubility of 6-MNA is higher at *p*H 7.4 and for piperazinyl prodrugs **(25a-25b** and **26a-26b)** it is higher at *p*H 5.0 Overall, substituted piperazinylalkyl prodrugs exhibited higher aqueous solubility as compared to 6-MNA **(16)** at *p*H 5.0. Aqueous solubility of all piperazinylalkyl prodrugs of 6-MNA at *p*H 7.4 was found to be comparatively lesser than 6-MNA.

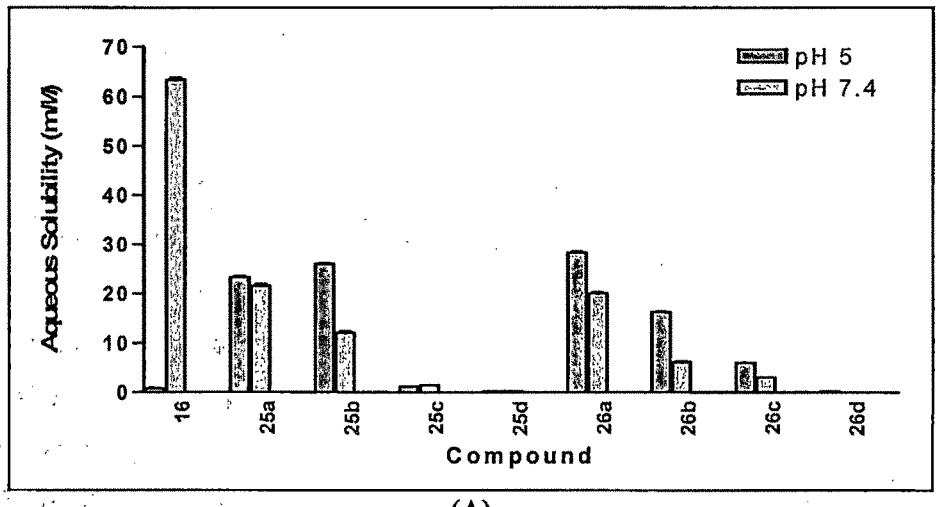

(A)

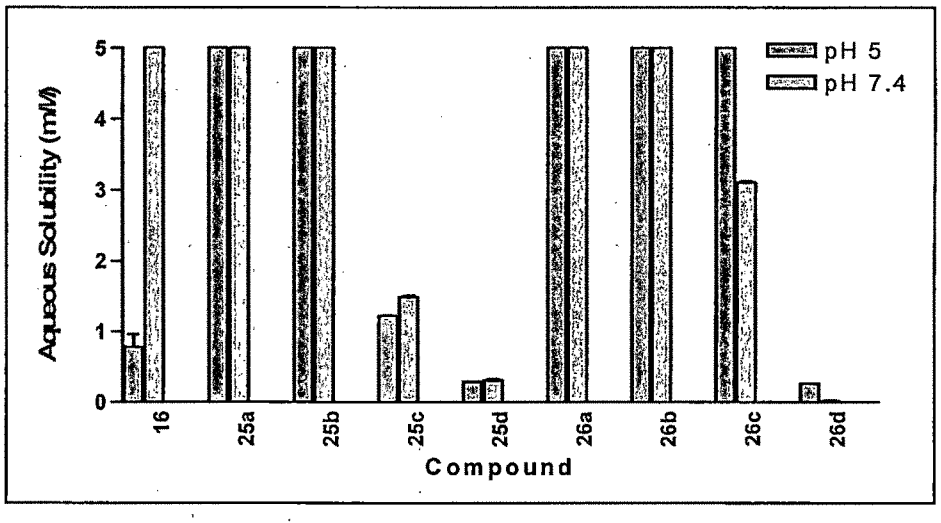

(B)

Fig. 3.2.18: **A**-Comparison of aqueous solubility at *p*H 5.0 and *p*H 7.4, **B**-expanded view scale 0-5 m*M* (Y axis). P<0.0001 compared to 6-MNA **(16)** (Bonferroni's test one way ANOVA)

The data showed that aqueous solubility of piperazinyl prodrugs was *p*H dependent and lowering the *p*H generally increased aqueous solubility of the prodrugs. Substituted piperazinyl promoieties seemed to be suitable for maintaining or increasing the aqueous solubility of 6-MNA at *p*H range 5.0 and *p*H 7.4.

3.2.2.2 Determination of apparent partition coefficient (Log P_{app})

Lipid solubility plays a crucial role in determining skin permeability of a particular compound because stratum corneum (SC) the major barrier to drug permeation is essentially lipoidal in nature and generally favors permeation of lipophilic drugs. The apparent partition coefficients of 6-MNA **(16)** and prodrugs were determined by partitioning them between phosphate buffer (0.16 M) and saturated *n*-octanol at *p*H 5.0 and *p*H 7.4 using shake flask method.

Although the partition domain of human SC lipids is more polar than octanol.[5-6] octanol is often used to estimate skin/water partition coefficient because the partionating in 1-octanol/water system mimics the partition in skin/water system.[7] The apparent partition coefficients of 6-MNA **(16)** and prodrugs are listed in **Table 3.2.12.**

All of the prodrugs of 6-MNA **(16)** have retained more or less comparable lipophilicity at pH 5.0 except derivative **(25d,** log P_{app}=2.171±0.005) which is more lipophilic than 6-MNA **(16)** (log P_{app}=1.823±0.002). At *p*H 7.4 all the prodrugs showed increased log P_{app} values as compared to 6-MNA with a maximum increase in lipophilicity of about 10 fold for prodrug **(26d)**

Table 3.2.12: Log P_{app} values of 6-MNA **(16)** and its prodrugs **(25a-25d and 26a-26d)**

Compound	Log P_{app}	
	***p*H 5.0**	***p*H 7.4**
16	1.823 ± 0.002	-0.233 ± 0.012
25a	0.104 ± 0.001	0.235 ± 0.001
25b	0.041 ± 0.001	0.434 ± 0.003
25c	1.217 ± 0.001	0.911 ± 0.001
25d	2.171 ± 0.005	1.164 ± 0.010
26a	0.119 ± 0.002	0.220 ± 0.007
26b	0.069 ± 0.005	0.539 ± 0.006
26c	0.372 ± 0.002	0.670 ± 0.001
26d	1.147 ± 0.003	2.04 ± 0.01

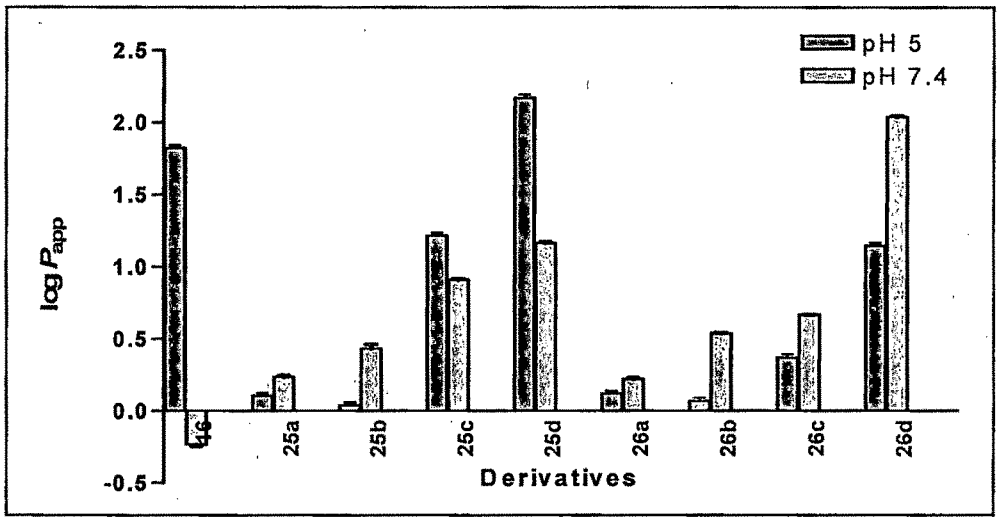

Fig. 3.2.19: Comparison of log P_{app} values at *p*H 5.0 and *p*H 7.4, P <0.0001 compared with 6-MNA **(16)** (Bonferroni's test one way ANOVA)

Although the lipophilicity of most of the prodrugs were lower at *p*H 5.0 than at *p*H 7.4 but some of them maintained good lipophilicity (logP_{app} = 0.04-2.17) at this pH (5.0). The lipophilicity of all the prodrugs of 6-MNA **(16)** varied widely due to changes in promoieties. For an effective dermal penetration, prodrugs should possess not only high lipophilicity but also adequate aqueous solubilities which is improved in this case by piperazinyl promoieties.

3.2.3 Hydrolyses kinetics studies

In addition to suitable aqueous and lipid solubility, percutaneous prodrugs should be stable chemically in bulk form and in dosage formulations. Thus, degradation of prodrugs was studied both at physiological *p*H 7.4 and in acidic *p*H 5.0 at constant temperature 37±1 ^{0}C. To determine the order of reaction three main methods are generally employed i.e. substitution method, half-life method and graphical method, The most commonly used method is graphical method, which is used here for determining the order of reaction.

3.2.3.1 Determination of order of reaction for derivative (25a) at *p*H 5.0

The data obtained for determining the order of reaction for prodrug (25a) at pH 5.0 is showed in **Tables 3.2.13-3.2.15**

Table 3.2.13: Data representation for calculation of rate constant (K) of derivative **(25a)** at *p*H 5.0 using zero order. Initial concentration **(y)** at 0 hours=**36.55 µg/ml**

Time (hrs)	Area (mVs)	Amt. degraded (x)	(y-x) (µg/ml)	(y-x) (mol/lit.)
0	7880	0	36.555	1.06×10^{-4}
12	7492	1.819	34.736	1.01×10^{-4}
48	5940	9.096	27.759	8.02×10^{-5}
60	5214	12.50	24.055	7.03×10^{-5}
72	4404	16.297	20.258	5.92×10^{-5}
84	3745	19.387	17.168	5.02×10^{-5}

Where, x = Concentration of the derivative (**25a**) which got hydrolysed at various time intervals.

(y-x) = Concentration of the derivative (mol/lit) (**25a**) left in the solution at various time intervals.

Table 3.2.14: Data representation for calculation of rate constant (K) of derivative **(25a)** at *p*H 5.0 using first (log y-x); second 1/(y-x) and third $1/(y-x)^2$ order.

Time (hrs)	Area (mVs)	(y-x) (µg/ml)	Log (y-x)	1/(y-x)	$(y-x)^2$	$1/(y-x)^2$
0	7880	36.555	-3.971	9355	1.142×10^{-8}	8.75×10^{7}
12	7492	34.736	-3.993	9845	1.031×10^{-8}	9.69×10^{7}
48	5940	27.459	-4.095	12454	6.446×10^{-9}	1.55×10^{8}
60	5214	24.055	-4.152	14216	4.947×10^{-9}	2.02×10^{8}
72	4404	20.258	-4.227	16882	3.508×10^{-9}	2.85×10^{8}
84	3745	17.168	-4.299	19920	2.519×10^{8}	3.97×10^{8}

Where, Log (y-x) = Logarithmic value of concentration of the derivative (**25a**) left in the solution at various time intervals.

Table 3.2.15: Order of reaction for derivative **(25a)** at *p*H 5.0

Order of reaction	**R^2**
Zero order	0.9489
First order	**0.9598**
Second order	0.9091
Third order	0.8422

So, from the value of R^2 it is apparent that the degradation kinetics of the compound **(25a)** followed first order because R^2 of first order is nearest to 1.

For first order half-life $t_{1/2} = 0.693/K$, where K = rate constant

From first order equation, $LogC = -Kt/2.303 + LogC_0$

From the first order graph, slope = $-K/2.303 = -0.0038$

$K = 0.00875$

$t_{1/2} = 0.693/K = 0.693/0.00875 = 79.18$ hr

3.2.3.2 Determination of order of reaction for derivative (25a) at *p*H 7.4

In a similar manner as described for derivative **(25a)** at *p*H 5.0, calculations were done at *p*H 7.4 for the reaction kinetics. The order of the reaction was determined and found out to be first order as shown in **Table 3.2.16.**

Table 3.2.16: Order of reaction for derivative **(25a)** at *p*H 7.4

Order of reaction	**R^2**
Zero order	0.6005
First order	**0.8685**
Second order	0.8038
Third order	0.5910

For the first order, half-life $t_{1/2} = 0.693/K$, where K = rate constant

From first order equation, $LogC = -Kt/2.303 + LogC_0$

From the first order graph, slop = $-K/2.303 = -0.0173$

$K = 0.03984$

$t_{1/2} = 0.693/K = 0.693/0.00875 = 17.39$ hr

Considering that the hydrolysis of the piperazinylalkyl ester derivatives followed first order degradation kinetics, further calculations were done for finding the rate constant (K) and hence half-life for other derivatives **(Table 3.2.17)** according to the first order kinetic equation i.e. $LogC = -Kt/2.303 + LogC_0$

The aqueous stability of piperazinyl prodrugs was *p*H dependent and stabilities were substantially greater at *p*H 5.0 than at *p*H 7.4. The reason for high instability at *p*H 7.4 is quite obvious as the esters are more prone to hydrolysis in alkaline medium due to higher concentration of hydroxide nucleophile.

3.2.3.3 Stability study in human serum

An essential prerequisite for the successful development of a percutaneous prodrug is its bioconversion to the drug in the skin. Distribution of esterases that are capable of hydrolyzing ester prodrugs are widespread in the body and several types of specific and non-specific esterases are found in blood and skin.[5-6] In the present study, the enzymatic hydrolysis kinetics study of prodrugs was carried out in human serum.

All prodrugs were found to be highly susceptible to enzymatic hydrolysis in human serum *in vitro*. They exhibited first order degradation kinetics and hydrolyzed quantitatively to the corresponding parent drugs. Half-life ($t_{1/2}$) values of prodrugs were summarized in **Table 3.2.17**

3.2.4 *In-vitro* skin permeation study

The diffusion experiments showed that both 6-MNA **(16)** and its prodrugs were able to permeate rat abdominal skin *in vitro*. For different prodrugs and for 6-MNA the cumulative amounts permeated through skin were plotted against time. A steady state flux (*J*ss) was obtained by dividing the slope of that graph by surface area of the diffusion cell.[1,8] The steady-state flux (*J*ss) of 6-MNA **(16)** and prodrugs were given in **Table 3.2.18.** All the prodrugs have shown higher flux values than the parent NSAID **(16).**

Table 3.2.17: Half-lives of the prodrugs in phosphate buffer at *p*H 5.0, 7.4 and in human Serum

Compound	Half-life ($t_{1/2}$)		
	Phosphate buffer ($t_{1/2}$ in hr)		Human serum (90%) ($t_{1/2}$ in min)
	*p*H 5.0	*p*H 7.4	
25a	79.18	17.39	46.29
25b	250.76	21.96	37.61
25c	27.60	27.86	< 10*
25d	< 6*	< 6*	ND
26a	376.14	23.50	60.18
26b	601.82	45.59	29.79
26c	158.3	30.39	< 10*
26d	< 6*	< 6*	ND

*complete disappearance of derivatives within this time interval, **ND**: Not done

Amongst all of the prodrugs, prodrug **(26b)** has shown the highest steady state flux and **(25b)** the lowest. Prodrugs **(25a)** and **(26a)** have shown intermediate flux values but both have shown 5-fold and 7-fold higher values than the parent NSAID. Prodrug **(26b)** having the highest flux was 12-fold higher than the parent NSAID. The results showed that lipophilic piperazinyl prodrugs with adequate aqueous solubility increased the flux of 6-MNA **(16)**.

Table 3.2.18: Steady state flux and permeability coefficient of 6-MNA **(16)** and prodrugs **(25a-25b** and **26a-26b)**

Compound	Permeability coefficient K_p	Steady state flux *Jss* ($\mu g/cm^2h$)
16	1.953	0.46
25a	0.356	2.23
25b	0.244	1.37
26a	0.286	2.98
26b	0.655	5.46

Table 3.2.19: Permeation profile data of **16** and derivatives **(25a-25b** and **26a-26b)**

Time (h)	Cumulative amount (µg)				
	16	**25a**	**25b**	**26a**	**26b**
1	3.85±0.60	21.33±0.80	13.11±0.90	25.28±1.60	37.52±1.40
2	5.81±0.90	30.54±1.10	18.79±1.30	43.67±2.40	95.95±4.50
4	16.01±1.10	85.46±1.60	51.43±2.30	109.56±4.70	196.35±8.90
8	29.49±1.50	148.97±3.10	96.54±4.50	201.04±5.90	310.45±12.30
12	31.80±1.80	178.69±5.60	104.55±5.30	235.81±9.60	384.14±18.99
24	37.96±10.0	210.33±12.31	131.65±6.10	283.61±18.47	560.44±32.13

The results clearly demonstrated that those prodrugs of 6-MNA **(16)** which possessed adequate lipid and aqueous solubility, permeated the skin better than those prodrugs which had low lipophilicity and poor aqueous solubility.

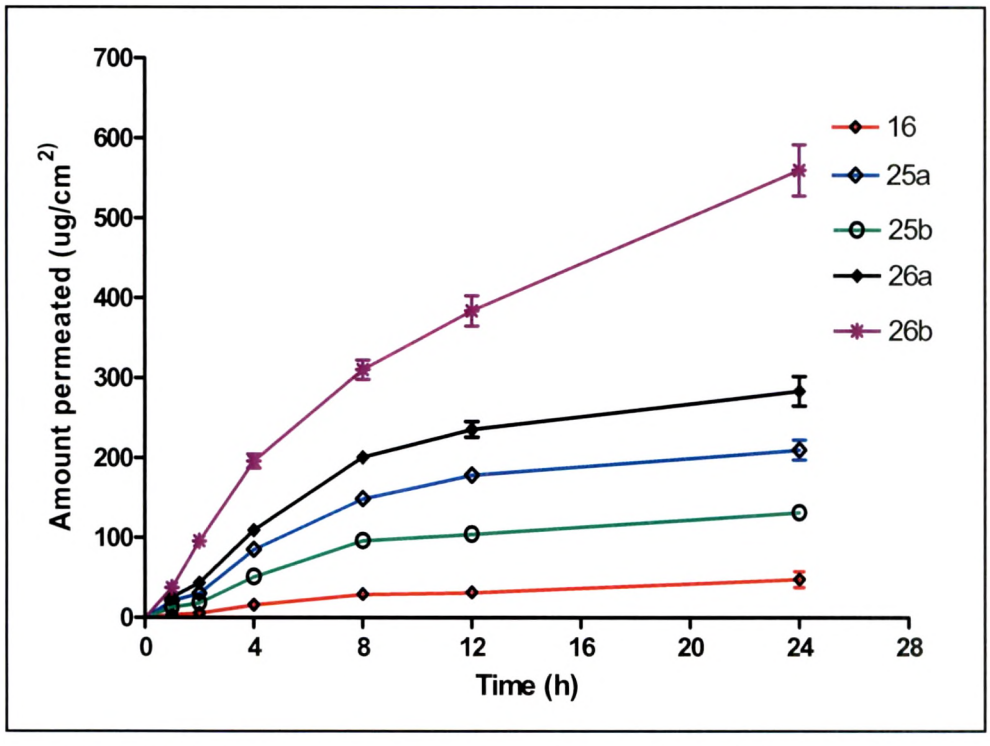

Fig. 3.2.20: Permeation profiles (mean SEM, n=3) for **16** and prodrugs **(25-25a-b and 26a-26b)**

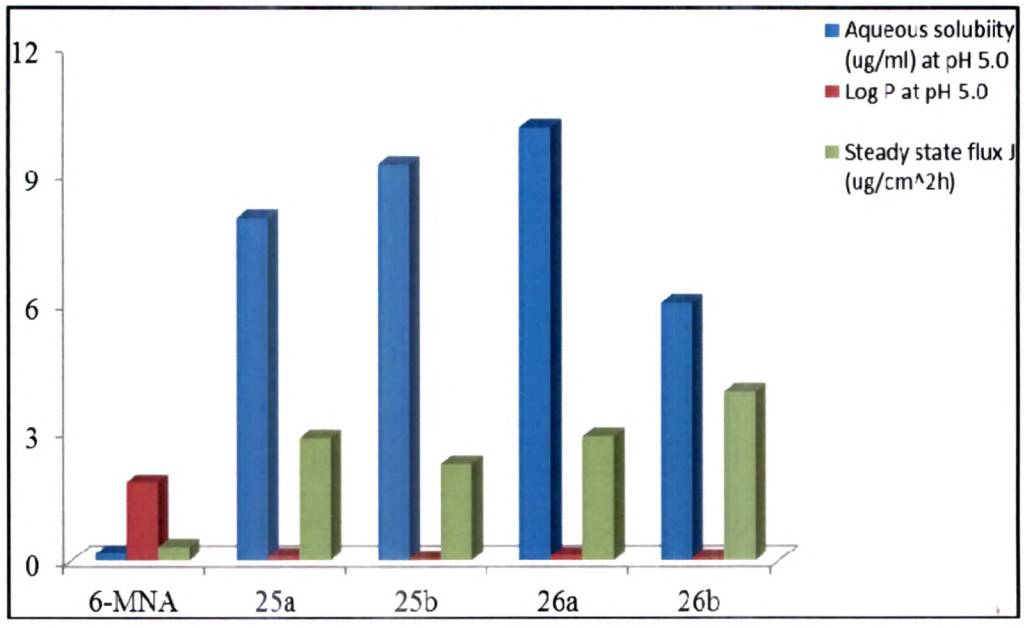

Fig. 3.2.21: Comparison of aqueous solubility, Log P_{app} and steady state flux (*J*ss) of 6-MNA **(16)** and derivatives **(25-25a-b** and **26a-26b)**

4. Experimental

All the reagents and solvents required for synthesis were purified by general laboratory techniques before use. Purity of the compounds and completion of reactions were monitored by thin layer chromatography (TLC) on silica gel plates (60 F_{254}; Merck), visualizing with ultraviolet light or iodine vapors. The yields reported here are un-optimized. Compounds were purified by column chromatography wherever required using neutral aluminum oxide (active) as stationary phase and suitable solvent as eluent.

Melting points were determined using a Veego make silicon oil bath-type melting point apparatus and are uncorrected. The IR spectra were recorded using KBr disc method in cm^{-1} on a Bruker FT-IR, Model 8300. The PMR and ^{13}C NMR (ppm) spectra were recorded in $CDCl_3$ on a Bruker 400 MHz spectrometer (chemical shifts in δ ppm, coupling constant *J* in MHz). λ_{max} was determined on Shimadzu 1800 UV spectrophotometer. HPLC analysis was performed by using Shimadzu prominence UV/VIS (pump LC-20AT, detector SPD 20 A), column purospher 5μ (e) C-18, 4.6 X 250 mm, Column temperature was 25-28 °C. Chromatography was performed under isocratic conditions, at a flow-rate of 0.9 ml/min. The mobile phase consisted of phosphate buffer (PB, 15 mM)-acetonitrile.

Mass of the compounds was determined in LCMS. *In vitro* skin permeation study was conducted using Franz type diffusion cell and Wistar rats were used as source of skin. Scanning electron microscope (SEM) model ESEM-EDAX XL-30, Philips (Netherlands) was used for surface morphology study.

The work carried out has been discussed under the following heads:

4.1 Chemical studies

4.1.1 Syntheses of salts

4.1.2 Syntheses of prodrugs

4.2 Physicochemical evaluation studies

4.2.1 Determination of aqueous solubility

4.2.2 Determination of partition coefficient (Log P_{app})

4.2.3 Hydrolysis kinetics studies

4.2.4 *In vitro* skin permeation studies

4.1 Chemical studies

4.1.1 Synthesis of salts

Equimolar amounts of the parent NSAID and amine/base were dissolved in dichloromethane under stirring and the stirring was continued for 2-4 h till the salts

precipitated out. Solvent was removed in *vacuo* and the residue was crystallized from methanol or ethyl acetate to get pure solid.

4.1.2 Synthesis of prodrugs

4.1.2.1. 2-Bromoethyl 2-(6-methoxy-2-naphthyl)acetate (22)

In a round bottom flask (250 ml), 6-MNA **(16)** (5.0 g, 23.14 mM) was dissolved in dry DCM (100 ml). The solution was cooled to 0-2 ^{0}C followed by the addition of EDC (5.30 g, 27.77 mM) in to it with stirring. DMAP (50 mg) was added into the reaction mixture as a catalyst followed by the slow addition of 2-bromothanol (4.90 ml, 69.44 mM). Stirring was continued till the reaction got completed.

After completion of the reaction (18 h), the reaction mixture was washed with chilled water (2 x 100 ml) to remove EDC and then with acetic acid (10 %, 2 x 50 ml) followed by washing with saturated solution of sodium bicarbonate (2 x 100ml) and again with chilled water (1 x 100 ml). DCM layer was separated and dried over anhydrous sodium sulphate, filtered and the solvent removed on rota evaporator to get a yellow product. Crude product so obtained was given charcoal treatment in methanol and recrystallized from methanol to get a fluffy white product. The solid product was dried in vacuum at 40 ^{0}C/300 mmHg (3.5 g, 46.79 %) m.p. 81-84 ^{0}C.

Anal.:

TLC (R_f) : 0.74 (Chloroform)

UV (MeOH) : 225 nm

IR (KBr, cm^{-1}): 1727 and 1214

PMR ($CDCl_3$): δ 7.71-7.67 (m, 3H, Ar-*H*), 7.39-7.37 (dd, 1H, Ar-*H*, *J*=1.76), 7.15-7.11 (m, 2H, Ar-*H*), 4.42-4.39 (t, 2H, -OC*H*$_2$, *J*=6.08), 3.91 (s, 3H, -OC*H*$_3$), 3.79 (s, 2H, -COC*H*$_2$) and 3.51-3.48 (t, 2H, -C*H*$_2$Br, *J*=6.08).

4.1.2.2. 2-(4-Methylpiperazin-1-yl)ethyl 2-(6-methoxy-2-naphthyl)acetate (25a)

Intermediate 2-bromoethyl 2-(6-methoxy-2-naphtyl)acetate **(22)** (0.5 g, 1.54 mM) was dissolved in dry acetone (20 ml) with DMF (two drop) in a pressure tube *N*-Methylpiperazine (0.46 g, 4.64 mM) and potassium carbonate (0.5 g, 3.62 mM) were added in the above reaction mixture. The tube was sealed and heated on oil bath at 70-80 ^{0}C with stirring. The reaction was monitored till completion (10 days) and the reaction mixture was filtered to remove K_2CO_3 and acetone recovered under vacuum to get brown

oily product which was purified by column chromatography using hexane: ethyl acetate (1:1) as the mobile phase and active neutral aluminium oxide as the stationary phase to yield yellowish brown oil which failed to crystallize. The oily product so obtained was dried in vacuum oven at 40 ^{0}C/300 mmHg (0.44 g, 83 %).

Anal.:

TLC (R_f) : 0.43 (Chloroform: Methanol; 9:1)

UV (H_2O) : 226 nm

IR (KBr, cm^{-1}) : 1730, 1264 and 1148

PMR ($CDCl_3$) : 7.63-7.03 (m, 6H, Ar-*H*), 4.16-4.13 (t, 2H, -OC*H*$_2$, *J*=5.8), 3.83 (s, 3H, -OC*H*$_3$), 3.68 (s, 2H, -OC*H*$_2$), 2.54-2.51 (t, 2H, N-C*H*$_2$, *J*=5.8), 2.38-2.27 (m, 8H, piperazine-*H*) and 2.16 (s,3H, -C*H*$_3$).

^{13}CNMR ($CDCl_3$): 171.67(1C, *C*O), 157.62-105.56 (10*C*, Ar-*C*), 62.31 (1C, OCH$_2$), 56.2 (O-*C*H$_3$), 55.3-54.94 (2C, piperazine), 52.93 (1C, -*C*H$_2$-N), 52.64-52.12 (2C, piperazine), 45.70 (Ar-*C*H$_2$-) and 41.20 (1C,-N-*C*H$_3$).

Mass (m/z) : 342.5 (M^+)

HPLC : > 98.9 %

4.1.2.3. 2-(4-Ethylpiperazin-1-yl)ethyl 2-(6-methoxy-2-naphthyl)acetate (25b)

Derivative (**25b**) was synthesized by the same procedure as mentioned for derivative (**25a**) using 2-bromoethyl 2-(6-methoxy-2-naphthyl)acetate (**22**) (0.5 g, 1.54 mM) and *N*-ethylpiperazine (0.21 g, 1.85 mM) to get an oily product which was purified by column chromatography using hexane: ethyl acetate (1:1) as the mobile phase and active neutral aluminium oxide as stationary phase. Yellowish green oily product so obtained was dried in vacuum oven at 40 ^{0}C/300 mmHg (0.25 g, 45.45 %).

Anal.:

TLC (R_f) : 0.53 (Chloroform: Methanol; 9:1)

UV (Distilled H_2O): 226 nm

IR (KBr, cm^{-1}) : 1731, 1264 and 1151

PMR ($CDCl_3$) :7.63-7.03 (m, 6H, Ar-*H*), 4.17-4.14 (t, 2H, -OC*H*$_2$, *J*=5.76), 3.83 (s, 3H, -OC*H*$_3$), 3.68 (s, 2H, -COC*H*$_2$), 2.54-2.52 (t, 2H, -C*H*$_2$N, *J*=5.76), 2.38-2.37 (m, 8H, piperazine-*H*), 2.31 -2.26 (q, 2H, -C*H*$_2$, *J*=7.2) and 0.99-0.95 (t, 3H, -C*H*$_3$, *J*= 7.16)

HPLC :> 96 %

4.1.2.4. 2-(4-Acetylpiperazin-1-yl)ethyl 2-(6-methoxy-2-naphthyl)acetate (25c)

Derivative (**25c**) was synthesized by the procedure as mentioned for derivative (**25a**) using 2-bromoethyl 2-(6-methoxy-2-naphthyl)acetate (**22**) (0.5 g, 1.54 mm) and *N*-acetylpiperazine (0.23 g, 1.84 mM) to get an oily product which was purified by column chromatography using hexane:ethyl acetate (1:1) as the mobile phase and active neutral aluminium oxide as stationary phase. The red brown oily product so obtained was dried in vacuum oven at 40 ^{0}C/300 mmHg (0.17 g, 34.88 %).

Anal.:

TLC (R_f)	: 0.56 (Chloroform: Methanol; 9:1)
UV (H_2O)	: 225 nm
IR (KBr, cm^{-1})	: 1730, 1626, 1263 and 1150
PMR ($CDCl_3$)	: 7.63-7.03 (m, 6H, Ar-*H*), 4.16-4.13 (t, 2H, -OCH_2, *J*=5.44), 3.82 (s, 3H, -OCH_3), 3.67 (s, 2H, -COCH_2), 3.13-3.11 (t, 2H, N-CH_2, *J*=5), 2.52-2.50 (m, 4H, piperazine-*H*), 2.29-2.19 (m, 4H, piperazine-*H*) and 1.90 (s, 3H, -COCH_3)
HPLC	:> 96 %

4.1.2.5. 2-(4-Phenylpiperazin-1-yl)ethyl 2-(6-methoxy-2-naphthyl)acetate (25d)

Derivative (**25d**) was synthesized by the same procedure as mentioned for derivative (**25a**) using 2-bromoethyl 2-(6-methoxy-2-naphthyl)acetate (**22**) (0.5 g, 1.54 mM) and *N*-phenylpiperazine (0.30 g, 1.85 mM to get a crude solid product which was successively recrystallized from methanol to yield white solid. The product was dried in vacuum oven at 60 ^{0}C/300 mmHg (0.3 g, 47.91 %) m.p. 91-93 ^{0}C.

Anal.:

TLC (R_f)	: 0.69 (Chloroform: Methanol; 9:1)
UV (H_2O)	: 226 nm
IR (KBr, cm^{-1})	: 1720, 1234 and 1147
NMR ($CDCl_3$)	: 7.70-7.22 (m, 6H, Ar-*H*), 7.15-6.80 (m, 5H, phenyl-*H*), 4.29-4.27 (t, 2H, -OCH_2, *J*=5.56), 3.90 (s, 3H, -OCH_3), 3.77 (s, 2H, -COCH_2), 3.02-2.95 (t, 4H, piperazine-*H*, *J*=5.08), 2.67-2.64 (t, 2H, N-CH_2, *J*=5.56) and 2.52-2.49 (t, 4H, piperazine-*H*, *J*= 5.12)
HPLC	: > 90 %

4.1.2.6. 3-Bromoproyl 2-(6-methoxy-2naphthyl)acetate (23)

In a round bottom flask (250 ml), 6-MNA **(16)** (1.0 g, 4.62 mM) was dissolved in dry DCM (100 ml). The solution was cooled to 0-2 ^{0}C followed by the addition of EDC (1.06 g, 5.55 mM) in to it with stirring. DMAP (50 mg) was added into the reaction mixture as a catalyst followed by the slow addition of 3-bromo-1-propanol (0.62 ml, 6.94 mM). Stirring was continued till the reaction was completed.

After completion of the reaction (18 h), the reaction mixture was washed with chilled water (2 x 50ml) to remove EDC and then with acetic acid (10 %, 2 x 25 ml) followed by washing with saturated solution of sodium bicarbonate (2 x 50 ml) and again with chilled water (1 x 50 ml). DCM layer was dried over anhydrous sodium sulphate and the solvent removed on rota evaporator to get a yellow product. The crude product so obtained was given charcoal treatment in methanol and recrystallized from methanol to get a fluffy white product. The solid product was dried in vacuum at 40 ^{0}C/300 mmHg (0.8 g, 51.25 %) m.p. 44-46 ^{0}C

Anal.:

TLC (R_f) : 0.81 (Chloroform)

UV (MeOH) : 225 nm

IR (KBr, cm^{-1}): 1735 and 1267

PMR ($CDCl_3$) : 7.71-7.68 (dd, 2H, Ar-*H*, *J*=4.28), 7.64 (s, 1H, Ar-*H*) 7.38-7.35 (m, 1H, Ar-*H*,), 7.15- 7.11 (m, 2H, Ar-*H*), 4.25-4.22 (t, 2H, -OCH_2, *J*=6.56), 3.91 (s, 3H, -OCH_3), 3.75 (s, 2H, -COCH_2), 3.40-3.36 (t, 2H, -CH_2Br, *J*=6.04) and 2.18-2.11 (m, 2H, -CH_2, *J*=6.56).

4.1.2.7. 3-(4-Methylpiperazin-1-yl)propyl 2-(6-methoxy-2-naphthyl)acetate (26a)

Derivative **(26a)** was synthesized by the same procedure as mentioned for derivative **(25a)** using intermediate 3-bromoproyl 2-(6-methoxy-2-naphthyl)acetate **(23)** (0.3 g, 0.890 mM) and *N*-methylpiperazine (0.106 g, 1.068 mM) to get brown oily product. The oily product was purified by column chromatography using hexane: ethyl acetate (1:1) as the mobile phase and active neutral aluminium oxide as the stationary phase to yield a brown oily product which failed to crystallize. The product so obtained was dried in vacuum oven at 40 ^{0}C/300 mmHg (0.15 g, 48.31 %).

Anal.:

TLC (R_f) : 0.60 (Chloroform: Methanol; 10:0.5)

UV (H_2O) : 226 nm

IR (KBr, cm^{-1}) : 1732, 1398 and 1163

PMR ($CDCl_3$) :7.63-7.03 (m, 6H, Ar-*H*), 4.07-4.04 (t, 2H, -OCH_2, *J*=6.48), 3.81 (s, 3H, -OCH_3), 3.64 (s, 2H, -COCH_2), 2.34-2.28 (m, 8H, piperazine-*H*), 2.27-2.23 (t, 2H, -NCH_2, *J*=7.24), 2.16 (s, 3H, N-CH_3) and 1.75-1.69 (m, 2H, -C-CH_2, *J*=7.04).

HPLC :> 97.5 %

4.1.2.8. 3-(4-Ethylpiperazin-1-yl)propyl 2-(6-methoxy-2-napthyl)acetate (26b)

Derivative **(26b)** was synthesized by the same procedure as mentioned for derivative **(25a)** using intermediate 3-bromoproyl 2-(6-methoxy-2naphthyl)acetate **(23)** and *N*-ethylpiperazine (0.12 g, 1.0 mM) to get brown oily product. The product was purified by column chromatography using hexane: ethyl acetate (1:1) as the mobile phase and active neutral aluminium oxide as stationary phase to yield brown oily product which failed to crystallize. The product so obtained was dried in vacuum oven at 40 ^{0}C/300 mmHg (0.20 g, 62.50 %).

Anal.:

TLC (R_f) : 0.40 (Chloroform: Methanol; 10:0.5)

UV (H_2O) : 226 nm

IR (KBr, cm^{-1}) : 1732, 1265 and 1156

NMR ($CDCl_3$) : 7.55-6.95 (m, 6H, Ar-*H*), 3.99-3.96 (t, 2H, -OCH_2, *J*=6.4), 3.75 (s, 3H, -OCH_3), 3.54 (s, 2H, -CH_2), 2.50-2.47 (t, 2H, N-CH_2), 2.42-2.26 (m, 8H, piperazine-*H*), 2.21-2.19 (m, 2H, -N-CH_2), 1.58-1.55 (m, 2H, -CH_2-, *J*=4.88) and 0.97-0.94 (m, 3H, -CH_3).

HPLC :> 90 %

4.1.2.9. 3-(4-Acetylpiperazin-1-yl)propyl 2-(6-methoxy-2-napthyl)acetate (26c)

Derivative **(26c)** was synthesized by the same procedure as mentioned for derivative **(25a)** using intermediate 3-bromoproyl 2-(6-methoxy-2-naphthyl)acetate **(23)** and *N*-acetylpiperazine (0.22 g, 1.78 mM) to get brown oily product which was purified by column chromatography using hexane: ethyl acetate (1:1) as the mobile phase and active neutral aluminium oxide as stationary phase to yield brown oily product which failed to crystallize. The product thus obtained was dried in vacuum oven at 40 ^{0}C/300 mmHg (0.51 g, 89.47 %).

Anal.:

TLC (R_f)	:	0.51 (Chloroform: Methanol; 19:1)
UV (H_2O)	:	226 nm
IR (KBr, cm^{-1})	:	1728, 1632, 1263 and 1150
NMR ($CDCl_3$)	:	7.70-7.11 (m, 6H, Ar-*H*), 4.17-4.13 (t, 2H, -OC*H*$_2$, *J*=6.4), 3.91 (s, 3H, -OC*H*$_3$), 3.73 (s, 2H, -COC*H*$_2$), 3.57-3.54 (t, 2H, N-C*H*$_2$, *J*=5.12), 3.38-3.35 (t, 2H, piperazine -*H*), 2.33-2.27 (m, 6H, piperazine-*H*) 2.05 (s, 3H, -COC*H*$_3$), 1.80-1.77 and (m, 2H, -C*H*$_2$, *J*=5.12)
^{13}C NMR ($CDCl_3$):		δ 171.76 (1C, -*C*O), 168.92 (1C, -*C*O), 157.65-105.56 (10C, Ar-*C*), 62.94 (1C, -O*C*H$_2$), 55.32 (1C, -O*C*H$_3$), 54.57 (1C, N-*C*H$_2$), 53.05-52.60 (2C, piperazine-*C*), 46.04 (1C, -*C*H$_2$CO), 41.50-41.18 (2C, piperazine-*C*), 25.80 (1C, -*C*H$_2$) and 21.31 (1C, -*C*H$_3$).
HPLC		:> 92.8 %

4.1.2.10. 3-(4-Phenylpiperazin-1-yl)propyl 2-(6-methoxy-2-naphthyl)acetate (26d)

Derivative (**26d**) was synthesized by same procedure as mentioned for derivative (**25a**) using intermediate 3-bromoproyl 2-(6-methoxy-2-naphthyl)acetate (**23**) and *N*-phenylpiperazine (0.28 g, 1.78 mM) to get crude solid product which was successively recrystallized from methanol to yield light brown solid. The product was dried in vacuum oven at 60 ^{0}C/300 mmHg (0.3 g, 48.32 %) m.p. 78-80 ^{0}C.

Anal.:

TLC (R_f)	:	0.73 (Chloroform: Methanol; 1:0.05)
UV (H_2O)	:	227 nm
IR (KBr, cm^{-1})	:	2959, 1736, 1267 and 1155
NMR ($CDCl_3$)	:	δ 7.63-7.15 (m, 6H, Ar-*H*), 7.07-6.75 (m, 5H, phenyl-*H*), 4.11-4.07 (t, 2H, -OC*H*$_2$, *J*=6.44), 3.81 (s, 3H, -OC*H*$_3$), 3.66 (s, 2H, -C*H*$_2$CO), 3.06-3.04 (t, 4H, piperazine-*H*, *J*=4.88), 2.43-2.40 (t, 4H, piperazine-*H*, *J*=5.04), 2.32-2.28 (t, 2H, N-C*H*$_2$, *J*=7.2) and 1.77-1.73 (m, 2H, -C*H*$_2$, *J*=7.64).
Mass (m/z)	:	418 (M^+)
HPLC	:	> 99.6 %

4.2. Physicochemical evaluation

Chemicals and Reagents

1. Phosphate buffer (15 mM): Monobasic potassium dihydrogen phosphate (KH_2PO_4, 1.026 g) was dissolved in distilled water to make the volume up to 500 ml. (Molecular weight of KH_2PO_4 = 136.08 g/mol).
2. Phosphate buffer *p*H 5.0 (0.16 M): Monobasic potassium dihydrogen phosphate (KH_2PO_4, 2.177 g) was dissolved in distilled water to make the volume up to 100 ml. and the *p*H of the solution was adjusted with 0.2 M sodium hydroxide.
3. Phosphate buffer *p*H 7.4 (0.16 M): Monobasic potassium dihydrogen phosphate (KH_2PO_4, 2.177 g) was dissolved in distilled water to make the volume up to 100 ml and adjusted the pH of the solution with 0.2 M sodium hydroxide to *p*H 5.0.
4. Phosphate buffer saline *p*H 7.4: Dibasic disodium hydrogen phosphate (Na_2HPO_4, 1.38 g), monobasic potassium dihydrogen phosphate (KH_2PO_4, 0.27 g) and sodium chloride (8.0 g) were dissolved in distilled water to make the volume up to 1000 ml.

4.2.1 Aqueous solubility

The aqueous solubility of 6-MNA, BPA and their salts or prodrugs were determined in phosphate buffer (0.16 M) at both *p*H 5.0 and 7.4 at room temperature. Excess amounts of each prodrug were added to phosphate buffer (0.5 ml). The mixtures were stirred and centrifuged at 6000 rpm for 5 min. The concentrations of each of the salt or prodrugs in their saturated solutions were analyzed by the HPLC. The *p*H of the solutions was held constant throughout the experiment.[1,8]

4.2.2 Apparent partition coefficient (Log P_{app})

The apparent partition coefficients (log P_{app}) of 6-MNA, BPA and their salts or prodrugs were determined at room temperature between 1-octanol and phosphate buffer (0.16 M) at *p*H 5.0 and 7.4 using shake flask method. 1-Octanol was saturated with phosphate buffer for 24 h by stirring vigorously before use. A known concentration of the compound in phosphate buffer was shaken with a suitable fixed volume of 1-octanol. After shaking, both the phases were separated by centrifugation at 6000 rpm for 5 min. The concentrations of the compounds in the buffer phase and in the 1-octanol phase were determined by HPLC. [1,8]

4.2.3 Hydrolysis kinetics study

Stability Study or the rates of chemical hydrolysis of prodrugs were studied in aqueous phosphate buffer solutions of *p*H 5.0 and *p*H 7.4 (0.16 M) at 37±1 ^{0}C. An

appropriate amount of prodrug was dissolved in phosphate buffer (5 ml) and the solutions were maintained at temperature 37±1 ^{0}C. At appropriate time intervals, samples were taken and analyzed for the remaining quantity of the prodrug by the HPLC. Prodrugs were found to degrade by first-order degradation kinetics. Half-lives ($t_{1/2}$) for the hydrolysis of the different prodrugs were calculated from the slope of the linear portion of the plotted logarithm of the remaining concentration of the prodrugs versus time.[1,8] The first order equation ($t_{1/2} = 0.693/k$) was used to calculate the half-lives.

4.2.4 *In vitro* skin permeation studies

In vitro skin permeation studies were performed by using rat skin. Samples of rat skin were obtained from the abdominal region of Wistar rat. Abdominal region of the rat was shaved using depilatory cream (*Anne French*, Wyeth pharmaceuticals Ltd.). Animal was euthanized by high dose of anesthetic ether and the abdominal skin was excised and thoroughly washed with phosphate buffer saline solution (*p*H 7.4). The skin surface (epidermal side) was cleaned with the aid of cotton impregnated with aqueous sodium lauryl sulphate (1 % w/v, 0.5 ml). The remaining fat in the dermal side was entirely removed by cotton impregnated with ether. The skin was washed with distilled water and dried well with clean and dry cotton.[1,8]

The *in vitro* skin permeation studies were carried out using the Franz-type diffusion cell. Skin specimens were rehydrated before being mounted in the diffusion cell. The receptor medium (0.05 M phosphate buffer saline solution of *p*H 7.4) was stirred and kept at 37±1 ^{0}C throughout the study. The compounds were applied as solutions in phosphate buffer of *p*H 5.0. At specified time intervals aliquots (0.5 ml) were withdrawn from the receptor compartment and replaced with fresh buffer. The drug concentrations were analyzed by HPLC.

The steady-state flux for 6-MNA **(16),** BPA **(17)** and their salts or prodrugs were determined by plotting the cumulative amount of the parent drug and the intact prodrug as measured in the receptor phase against time, and dividing the slope of the steady-state position by the surface area of the diffusion cell (4.906 cm^2).[1,8] The permeability coefficients (K) for the steady-state delivery were obtained by dividing the steady-state flux by the solubilities of the compounds in the applied corresponding vehicle.

References

1. Rautio J., Nevalainen T., Taipale H., Vepsäläinen J., Gynther J., Laine K. and Järvinen T., Piperazinylalkyl prodrugs of naproxen improve *in vitro* skin permeation. *Eur.J. Pharm. Sci.*, **2000**, 11, 157-63
2. QikProp, version 3.2, Schrödinger, LLC, New York, NY, **2009**
3. Epik, version 2.0, Schrödinger, LLC, New York, NY, **2009**
4. Siddiqui O., Physicochemical physiological and mathematical consideration in optimizing percutaneous absorption of drugs. *Crit. Rev. Ther. Drug Carr. Syst.* **1989**, 6, 1-38
5. Anderson B.D., Higuchi W.I. and Raykar P.V., Heterogeneous effects on permeability partition coefficient relationship in human stratum corneum. *Pharm. Res.* **1988**, 5, 566-72
6. Raykar P.V., Fung M.C. and Anderson B.D., The role of protein and lipid domains in the uptake of solutes by human stratum corneum. *Pharm. Res.* **1988**, 5, 140-50
7. Williams F.M., Clinical significant of esterase in man. *Clin. Pharmacokin.***1985**, 10, 392-403
8. Amjad Q. and Soraya A. Synthesis of piperazinylalkyl ester prodrugs of ketorolac and their i*n vitro* evaluation fo,r transdermal delivery. *Drug. Dev. Ind. Pharm.* **2008**, 34, 1054-63
9. Singh S. and Singh J., Transdermal drug delivery by passive diffusion and iontophoresis: A Review. *Med. Res. Rev.*, **1993**, 13, 569-621.